DOI：CNKI:11-3841/TP.20130311.1705.009 网络出版时间：2013-03-11 17:05
网络出版地址：http://www.cnki.net/kcms/detail/11.3841.TP.20130311.1705.009.html

A priori knowledge application in the retrieval of surface albedo using HJ-1 CCD data

ZHANG Hu, JIAO Ziti , LI Xiaowen, HUANG Xingying, DONG Yadong

1. *School of Geography, Beijing Normal University, Beijing* 100875, *China*;
2. *State Key Laboratory of Remote Sensing Science Jointly Sponsored by Beijing Normal University and the Institute of Remote Sensing and Digital Earth, Chinese Academy of Sciences, Beijing* 100875, *China*;
3. *Key Laboratory of Environmental Remote Sensing and Digital City, Beijing* 100875, *China*

Abstract: This paper estimated HJ-1 land surface albedos in the Heihe region using the backup algorithm of Moderate Resolution Imaging Spectroradiometer (MODIS) Bidirectional Reflectance Distribution Function (BRDF)/Albedo product (method Ⅰ), the Bayesian inference-based algorithm (method Ⅱ) and the Lambertian surface algorithm (method Ⅲ). Compared inversed albedos with surface observations, statistical analysis results showed that: (1) The high resolution albedos from HJ-1 CCD data can provide spatial distribution of underlying surface as well as surface details. Different land cover types' statistic values indicates that method Ⅰ and method Ⅱ capture similar results, with the absolute error of 0.01 and the relative error of 4% as compared with albedos from MODIS, while method Ⅲ has the absolute error of 0.03 and relative error of 13%.(2) The improvement in the albedo by method Ⅰ and method Ⅱ is almost independent to land cover types, capturing relative error between 2% and 8%; However, the temporal reliance of estimated albedo is more significant, and the improvement is more obvious in the maturity than in the dormancy. (3) Surface albedos estimated by method Ⅰ and method Ⅱ have better consistency with field observations.The root mean square errors are less than 0.05, and relative errors are less than 23%, while results of method Ⅲ are 0.069 and 36.3%, respectively. (4) The retrieval of albedos based on the prior knowledge may depend on the geometry of the sun and the observation, and thus depend on the season and the latitude, as well as sensor specifications. This study will provide significant understanding for spaceborne albedo retrieval which lacks of sufficient multi-angular observations.

Key words: HJ-1 satellite, MODIS, BRDF, albedo, Bayes, priori knowledge

CLC number: TP701 **Document code**: A

Citation format: **Zhang H, Jiao Z T, Li X W, Huang X Y and Dong Y D. 2013. A priori knowledge application in the retrieval of surface albedo using HJ-1 CCD data. Journal of Remote Sensing, 17(2): 286-307**

1 INTRODUCTION

Land surface albedo is one of the key parameters in the surface radiation budget, the long range weather forecasting and global change researches. It has great significance for the study of global and regional climate models (Dickinson, 1995). Albedo is defined as the ratio of reflected radiation from the surface to incident radiation upon it (Nicodemus, et al., 1977). BRDF shapes of different land cover classes are variable (Strugnell & Lucht, 2001; Jin, et al., 2003), and accurate estimation of surface albedo from satellite data needs to consider the impact of surface reflectance anisotropies.

The satellite observations made the measurements available at both regional and global scales, but the data are still limited because of the noise and angular samplings. At present there are mainly three ways to estimate surface albedos from limited observations:

Method Ⅰ is based on the backup algorithm of MODIS BRDF/albedo (Strugnell, et al., 2001). Early researches about Very High Resolution Radiometer (AVHRR) show that this method considers the surface anisotropy to improve surface albedo retrieval accuracy (Strugnell & Lucht, 2001; Strugnell, et al., 2001). At present the archetypal BRDF shapes of this method have been associated a priori with each pixel globally (Schaaf, et al., 2002). Compared the backup inversed albedos and full inversed ones with field measurements, the result showed that there is little difference between these two methods (Jin, et al., 2003; Salomon, et al., 2006; Liu, et al., 2009).

Method Ⅱ is based on the Bayes inference theory. It takes field measured data sets as a priori knowledge (Li, et al., 2001). The method is dependent on a priori estimates of model parameters and their covariance matrix of the surface observation data. We can use a maximum likelihood algorithm to minimize a cost function to get the Bayesian maximum likelihood solution. The method is applicable for the data that has limited angular samplings, and it overcomes the shortcoming of the large amount of prior knowledge in the MODIS backup algorithm. It provides a new theoretical framework for the

Received: 2011-08-01; **Accepted**: 2012-06-14

Foundation: Natural Science Foundation of China (No.40871193,41171261); The Special Foundation for Free Exploration of State Laboratory of Remote Sensing Science (No.610ZY-06); Key Projects in the National Science & Technology Pillar Program (No.2008BAC34B03)

First author biography: ZHANG Hu (1986—), male, master, he majors in the research and application of quantitative remote sensing, surface bidirectional reflectance and surface albedo. E-mail: askzhanghu@126.com

Corresponding author biography: JIAO Ziti (1970—), male, Ph.D., associate professor. His research interests are modeling reflectance anisotropy and albedo, and differentiating land covers with multiple-view-angle remotely sensed data. He has published over 20 papers. E-mail: jiaozt@bnu.edu.cn

establishment of global BRDF database as well as the global BRDF and albedo retrieval. The main problem for this method may be the accumulation of the prior BRDF knowledge and how to constrain the prior knowledge (hard boundary, δ boundary and soft boundary).

Method Ⅲ is based on Lambertian assumption. It takes the single direction of observation data as the surface albedo. This method does not consider the influence of surface anisotropy and does not conform to the characters of anisotropic surface. Kimes' early research showed that Lambertian assumption can result in errors up to 45% (Kimes, 1985).

Information of remote sensing observations is always limited, and the priori knowledge is the key factor to solve the problem. The priori knowledge accumulation and application is necessary to improve the retrieval accuracy of the surface parameters (Li, et al., 2001). Estimating land surface albedos based on a priori knowledge has attracted more and more attention. Li (1998) described the important role of a priori knowledge in model inversion and fitting the field observations by using the kernel-driven BRDF model to obtain the model parameters, which was considered as a priori knowledge database of the surface BRDF (Li, et al., 2001). Pokrovsky (2002) used a statistical inversion method for inversion of BRDF models; The MODIS BRDF and albedo magnitude algorithm is based on a priori land surface BRDF database (Strugnell & Lucht, 2001); Wang (2007) proposed a regularizing kernel-based BRDF model inversion method that can apply to the data that has a limited angular sampling or a high degree of linear correlation as well as noise influences.

The main objective of this paper is to estimate land surface albedos from HJ-1 CCD data. Based on the kernel-driven BRDF model (RossThick-LiSparse-Reciprocal) (Lucht, et al., 2000), we used the backup algorithm of MODIS BRDF / albedo (method I), the method based on Bayes inference theory (method Ⅱ), and the Lambertian assumption algorithm (method Ⅲ) to inverse surface albedos, respectively. At last we compared the inversion results with albedo from MODIS and the field observations, and analyzed the differences among the estimated albedos. This research can provide some basis theory for the new method and for the production of regional high-resolution albedo products.

1.1 Introduce to study area

The study area is located in the upper areas of the Heihe region, the middle of Hexi Corridor, including Zhangye City and the surrounding oasis and part of Qilian Mountain. Natural variation is obvious within the region, where the mountain, vegetation and desert own distinct landscape areas and land cover changes obviously with the seasons. Inversing the albedo of this area has great significance. Elevation of the study area is about 1500 m. Four kinds of land cover types including woodland, grassland, cropland, bare land occupy more than 95% of the total area. There is a flux tower in the cropland near Yingke oasis station. It can provide the shortwave broadband surface albedos (Ma, et al., 2008).

1.2 Data Processing

Data used in this research included HJ-1 CCD data, MODIS products (BRDF/albedo product MCD43, aerosol product MOD04, global land cover dynamics product MCD12Q2), 73 sets of field observations (Hu, et al., 1997; Strugnell, et al., 2001; Li, et al., 2001), flux tower measurements and land cover data of Heihe region.

HJ-1 CCD data were obtained by four CCD cameras on HJ-1A and HJ-1B satellites. Each satellite could provide a swath width of 700 km with a spatial resolution of 30 m. The observation cycle is two days. Differing from the Landsat TM, HJ-1 CCD camera can provide the maximum viewing zenith angle of 35°. Fig.1 shows the spatial distribution of the sun and the observation geometry of a pixel in the study area in June. It can be seen from the Fig. 1 that HJ-1 A and B can provide 14 direction observations in one month, and these observations mainly distributes on the principle plane and can represent the anisotropic characteristics of the surface. But Fig. 1 did not consider the quality of the observations. Due to the effect of cloud or other reasons, it is hard to use all of the observations in practical model inversion. Atmospheric correction of HJ-1 CCD images was used with 6S algorithm. Validation results show that for grass and bare soil, this method yielded an average error of 8% in the red band and 35% in the near-infrared band (Sun, et al., 2010). For wheat, this method leaded to an error of 3% in the near-infrared band (Du, et al., 2010). CCD data used in this study don't have obvious clouds in the study area. We used the average value of MODIS aerosol product (MOD04) as aerosol optical thickness. Compared the spectroradiometric (Wang, et al., 2009) and Normalized Difference Vegetation Index (NDVI) of different land covers before and after calibration, the results showed that this method can effectively eliminate the effect of the atmosphere, and the error in atmospheric correction in the study area should be less than 10%. Land cover data was obtained by comprehensive HJ-1 B-CCD2 data on May 22nd, 2009 and landusemap of the study area.

MODIS is a key instrument aboard National Aeronautics and Space Administration's (NASA) Terra and Aqua satellites and provides global BRDF/albedo products. The MODIS BRDF/Albedo algorithm makes use of corrected multi-angle, multi-spectral data to provide land surface albedo products every 16 days (Schaaf, 2002, 2011). A lot of works have been done to validate MODIS land surface reflectance and albedo products (Liang, et al., 2002; Jin, et al., 2003; Salomon, et al., 2006; Liu, et al., 2009). Results showed that the absolute accuracy of the broadband albedo is about 0.02 to 0.05. At present, estimating the albedo from single direction and high resolution data also use MODIS products as a priori knowledge (Shuai, et al., 2011). In this research, MODIS data provides a priori knowledge of surface anisotropy for method I. According to the lati-

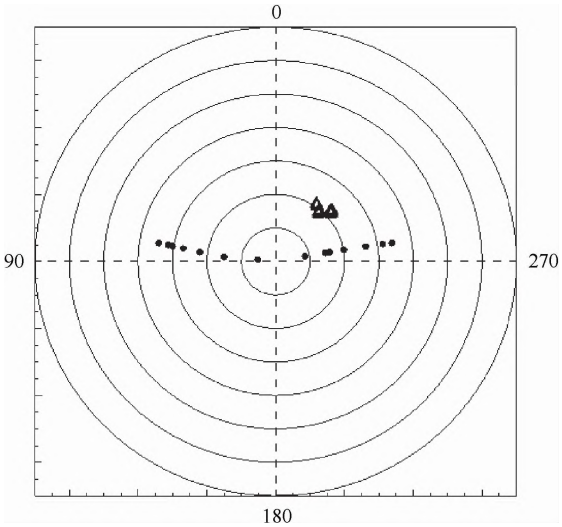

Fig.1 HJ-1 angular sampling in June 2009

(The radius represents the zenith angle with an interval of 10° and the polar angle represents the azimuth. Solid circles refer to the viewing direction and the open triangles refer to the location of the sun)

tude and longitude, we used the MODIS Reprojection Tool (MRT) to obtain the MODIS albedo products of the study area, and used the nearest neighbor algorithm to resample the data to 30 m resolution. HJ-1 CCD and MODIS band characteristics are shown in Table 1.

Table 1 Sensor character of MODIS and HJ CCD

Sensor		MODIS		HJ CCD	
Spatial resolution		500 m		30 m	
Spectral range	Band name	Band	Interval/nm	Band	Interval/nm
	Blue	3	459—479	1	430—520
	Green	4	545—565	2	520—600
	Red	1	620—670	3	630—690
	Nir	2	841—846	4	760—900

73 sets of field observations provide a priori knowledge for method Ⅱ. They were collected from many different sources, covering a large variety of land cover types. Most of these datasets are from PARABOLA radiometer measurements (Deering, et al., 1986) in FIFE and BOREAS campaigns. Some other datasets were from radiometer measurements by Kimes (Kimes et al., 1985, 1986), Ranson (Ranson, et al., 1985), and Irons (Irons, et al., 1992). There were also AVHRR data, airborne POLDER data (Leroy, et al., 1996) and scanning cloud absorption radiometer (SCAR) data (Tsay, et al., 1998). These datasets were acquired in the red and near infrared bands, and most of them were used for validating the models' fitting capabilities (Li, et al., 2001; Hu et al., 1997). We used the RossThick-LiSparse-Reciprocal (RTLSR) BRDF model fit those observations and smooth noise samples (Li, et al., 2001), excluding the data that have large fitting error. Finally, 69 datasets were used in this study.

Yingke oasis station is located in the farmland of Zhangye in GanSu province with a longitude of 100°25′E, latitude of 38°51′N and an altitude of 1519 m above sea level. Equipment of automatic meteorological measurements at the Yingke oasis station continuously observes and records 305—2800 nm hemisphere upward and downward radiance energy. After processing there is an observation every ten minutes (Ma, et al., 2008). In this study, the 20-min (around the time of HJ-1 passing over the study area) field observation albedos were averaged from the measurements, and then they were used for the albedo comparison.

2 METHOD BASED ON A PRIORI KNOWLEDGE

In this section, we first overviewed the semi-empirical kernel driven BRDF models, and then presented a brief introduction to the backup algorithm (method I) of MODIS albedo and algorithm based on Bayesian inference (method Ⅱ), and finally summarized the comparison of the inversion results between the different methods.

Semi-empirical kernel driven BRDF models are expanded into a linear sum of kernels, characterizing different scatting modes. This model was mathematically described as the linear combination of the isotropic kernel, volume scattering kernel and surface scattering (Roujean, et al., 1992; Wanner, et al., 1995; Lucht, et al., 2000).

$$R(\theta_i,\theta_r,\varphi) = f_{iso}(\lambda) + f_{vol}(\lambda)K_{vol}(\theta_i,\theta_r,\varphi) + f_{geo}(\lambda)K_{geo}(\theta_i,\theta_r,\varphi) \quad (1)$$

where R is the surface bidirectional reflectance, and K_{vol} represents the volume scattering kernel caused by a horizontal layer of randomly distribution leaves, and K_{geo} represent the surface scattering kernel caused by shadows of natural objects. They are the functions of viewing and illumination geometry; θ_i, θ_r, and φ are the solar zenith, view zenith and relative azimuth angles; $f_{iso}(\lambda)$, $f_{vol}(\lambda)$ and $f_{geo}(\lambda)$ are the spectrally dependent BRDF kernel weights or parameters. Kernels are only the functions of solar and sensor geometry, so we can get their integrals in advance. BSAs and WSAs are calculated by integrating the kernel value over the reflected radiation hemisphere or both the reflected and incident radiation hemisphere (Nicodemus, et al., 1977; Lucht, et al., 2000). Black and White sky albedos are defined in the ideal condition, and the combination of the two albedos can describe the real surface albedo (Lewis & Barnsley, 1994).

$$\alpha(\theta_i) \approx [1 - S(\tau)]\rho_{bs}(\theta_i) + S(\tau)\rho_{ws} \quad (2)$$

where $S(\tau)$ is the proportion of the diffuse skylight, it is a function of the aerosol optical depth τ. Excepting the large solar zenith angle condition, Eq.(2) can get the surface true albedo approximately.

2.1 Method I-based on the MODIS backup algorithm

Method Ⅰ is based on the MODIS backup algorithm which based on the surface BRDF shape archetype. The basic theory is assuming that interclass BRDFs are broadly similar and that differences are one of degree, rather than substantial changes in the shape of the BRDF function. We can use the BRDF shape archetype to fit the BRDF to the observations and to retrieve surface albedo (Strugnell, et al., 2001; Jin, et al., 2003). In this method we introduced the MODIS albedo product MCD43A1 as a priori knowledge of surface anisotropy. Using MCD43A1 and RTLSR model, we can obtain surface reflectance at any viewing and illumination geometry conditions. When the sensor provides enough observations, we can fit the BRDF archetype to observations by the least-squares fitting method, and hence get surface albedo. Obviously, for the HJ-1 CCD data, there is only one observation for each image, so we can't use the least squares method to find the closest solution. However, we can assume that the BRDF shapes of MODIS and HJ-1CCD data are broadly similar and that differences are one of degree rather than strict demarcation. Hence, we may define the relationship of surface BRDFs between MODIS and HJ by $BRDF_{hj} = a \times BRDF_m$, where $BRDF_m$, is the MODIS BRDF and $BRDF_{hj}$ represents the HJ-1 BRDF associated with MODIS BRDF, a is a multiplicative factor, which is used to generate a similar BRDF from MODIS by considering the changes in directional effects, it fellows that $a = \rho_0/\rho_s$, ρ_0 is the HJ CCD observations and ρ_s, which has the same observation condition with ρ_0, is the direction reflectance of MODIS. In this method the MODIS BRDF product is taken as a priori knowledge of underlying surface anisotropy and improves the accuracy of the albedo, and the value of the surface albedo depends on the HJ-1 CCD observation.

2.2 Method Ⅱ-based on Bayesian inference

Method Ⅱ is based on Bayesian inference. When the observations are limited or poor angular sampling, application of a priori knowledge is necessary. Through prior knowledge accumulation and application, Bayesian inference is the basic theory and ideal method to solve the uncertainty problem. This method takes model parameters as random variables, which have some kind of prior distribution, and uses maximum likelihood estimation method to infer posterior distribution of the parameters (Li, et al., 2001). Prior knowledge is not relation to a particular land cover type, it fits the prior knowledge to observations, and surface albedo inversion.

In practice, a simpler approach uses a maximum likelihood estimation that minimizes a cost function (Tarantola, 1987; Rodgers,

1976):

$$\mathrm{Cost}(\boldsymbol{X}) = (\boldsymbol{A}_{\mathrm{obs}}\boldsymbol{X} - \boldsymbol{Y}_{\mathrm{obs}})^{\mathrm{T}}\boldsymbol{C}_{\mathrm{d}}^{-1}(\boldsymbol{A}_{\mathrm{obs}}\boldsymbol{X} - \boldsymbol{Y}_{\mathrm{obs}}) + (\boldsymbol{X} - \boldsymbol{X}_0)^{\mathrm{T}}\boldsymbol{C}_{\mathrm{p}}^{-1}(\boldsymbol{X} - \boldsymbol{X}_0) \quad (3)$$

where $\boldsymbol{A}_{\mathrm{obs}}$ is the kernel matrix, $\boldsymbol{C}_{\mathrm{d}}$ is the noise covariance matrix of data noise and model inaccuracy, $\boldsymbol{C}_{\mathrm{p}}$ is the covariance matrix of prior knowledge of $\boldsymbol{X}_{\mathrm{obs}}$, $\boldsymbol{X}_0$ is the prior best guess of the vector $\boldsymbol{X}$. Here we take the mean of the model parameter derived from 69 data sets. Table 1 shows prior knowledge distribution for parameters of kernel driven model.

Table 2 Prior knowledge distribution for parameters of kernel driven model

	Red			Nir		
Parameter	f_{iso}	f_{vol}	f_{geo}	f_{iso}	f_{vol}	f_{geo}
Mean	0.1064	0.0508	0.0159	0.2892	0.1721	0.0295
Variance	0.0108	0.0028	0.0006	0.0091	0.0054	0.0012
covariance	0.00935	0.00137	0.00155	0.00773	0.00014	0.00160
	0.00137	0.00170	0.00034	0.00014	0.00959	−0.00235
	0.00155	0.00034	0.00045	0.00160	−0.00235	0.00145

The total $\mathrm{Cost}(\boldsymbol{X})$ thus consists of two parts, including the cost of data misfit and the cost of parameter deviation from the prior best guess. In the case that we don't have knowledge of $\boldsymbol{C}_{\mathrm{d}}$, so, as an alternative, we may add an artificial weight to the real observation part of the cost function (Li, et al., 2001):

$$\mathrm{Cost}(\boldsymbol{X}) = n(\boldsymbol{A}_{\mathrm{obs}}\boldsymbol{X} - \boldsymbol{Y}_{\mathrm{obs}})^{\mathrm{T}}(\boldsymbol{A}_{\mathrm{obs}}\boldsymbol{X} - \boldsymbol{Y}_{\mathrm{obs}}) + (\boldsymbol{X} - \overline{\boldsymbol{X}})^{\mathrm{T}}\boldsymbol{A}_{\mathrm{simu}}^{\mathrm{T}}\boldsymbol{A}_{\mathrm{simu}}(\boldsymbol{X} - \boldsymbol{X}_0) \quad (4)$$

The least squares solution is (Yang, et al., 2003):

$$\boldsymbol{X} = (n^2\boldsymbol{A}_{\mathrm{obs}}^{\mathrm{T}}\boldsymbol{A}_{\mathrm{obs}} + \boldsymbol{C}_{\mathrm{p}}^{-1})^{-1}\begin{bmatrix} n\boldsymbol{A}_{\mathrm{obs}} \\ \boldsymbol{A}_{\mathrm{simu}} \end{bmatrix}\begin{bmatrix} n\boldsymbol{y}_{\mathrm{obs}} \\ \boldsymbol{Y}_{\mathrm{simu}} \end{bmatrix} \quad (5)$$

where $\boldsymbol{\Lambda}$ is the diagonal matrix of eigenvalues and $\boldsymbol{E}$ is the corresponding matrix of column eigenvectors, $\boldsymbol{C}_{\mathrm{p}} = \boldsymbol{E}\times\boldsymbol{\Lambda}\times\boldsymbol{E}^{\mathrm{T}}$, $\boldsymbol{A}_{\mathrm{simu}} = \boldsymbol{\Lambda}^{-1/2}\times\boldsymbol{E}^{\mathrm{T}}$, $\boldsymbol{Y}_{\mathrm{simu}} = \boldsymbol{A}_{\mathrm{simu}}\times\boldsymbol{X}_0 = \boldsymbol{\Lambda}^{-1/2}\times\boldsymbol{E}^{\mathrm{T}}\times\boldsymbol{X}_0$, the weight n can be easily introduced into the standard linear regression. The weight actually depends on how much we trust the new observation and how much we trust the prior knowledge. The larger the n is, the closer the solution $\boldsymbol{X}$ will be drawn to the solution plan and the farther it will be from $\boldsymbol{X}_0$, however, it will be less stable. Therefore, there exists an appropriate value that can make the inversion result stable, while also keeping more observation information in the inversed parameters. To get the accurate ratio, Li, et al. (2001) select a well sampled data, and took the albedo from a full data set as the true value, then compared their direction observation inversion results with the true values for different priori ratios. He indicates that for a single-look inversion problem, a priori information ratio of 3/4 can get rather stable posterior estimates. We calculated the HJ-1 and MODIS WSA using different priori ratios and found when n changes in 1, it will cause a change about 0.02 in HJ-1 WSA, and when the values of n is around 9, the two WSAs are most similar.

Fig.2 shows two inversion methods of surface's albedos based on the priori knowledge. In order to validating the different results, we also calculated the surface's albedos based on the surface Lambertian assumption and MODIS broadband albedo at the time when HJ-1 passes over the study area. The surface's albedos based on the assumption of surface Lambert, simply equal to those directional reflectance (Liang, et al., 2001), MODIS broadband albedos can be obtained from their products. Considering the characteristics of seasonal variance of the surface, we chose several temporal HJ-1 CCD data of the study area to inverse the surface albedo. The temporal feature of the study area can be derived from the MODIS products (MCD12Q2) of the land surface penology, and the statistics results of the Enhanced Vegetation Index (EVI) showed that, surface types in the study area showed obvious seasonal changes. From mid April, the vegetations begin to grow, and mature in early July, and EVIs have the biggest values. Deciduous forest begins to senescence in late August. We totally select 13 HJ CCD data of different days which are less cloudy and high visible for surface albedo retrieval, and make a comparative analysis of the results for the typical phenology.

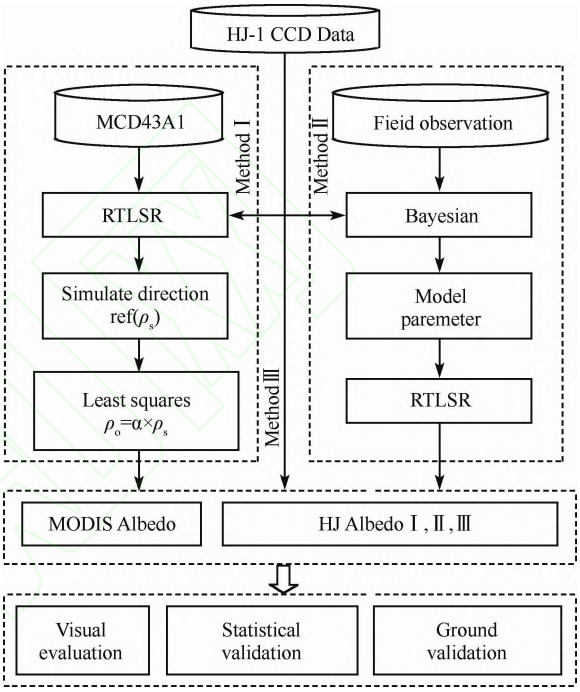

Fig.2 Flowchart of an algorithm for inversing surface albedo and results compare

3 RESULT AND ANALYSIS

To validate the accuracy of the inverse results, we evaluate the albedos acquired by the HJ CCD in the following methods. First, visually evaluate the surface albedos acquired by the two methods (method Ⅰ and method Ⅱ) with the production of MODIS albedos. Secondly, calculate the mean and variance of different land cover types, and compare the absolute and relative error of them. At last, compare the result acquired by the three methods with the production of MODIS and the ground observation data acquired by field observations. The ground observation data and the data of the HJ-1 CCD are the combination of direct and scattering light. In order to compare the two kinds of data directly, we consider the condition of atmosphere to translate the black and white sky albedo into the real albedo, and finally into the albedo with similar spectral range using the Eq. (2) to reduce the influence of the difference of spectral resolution. The ground-based 73 groups of observation data have only two bands: red band and near infrared band. The HJ CCD has a similar spectral range with the AVHRR. So we consult the transition coefficient in the procedure from narrow band to board band (Liang, et al., 2003).

3.1 Result and Statistics

Fig. 3 shows the distribution of shortwave broadband albedo

acquired by different methods in Heihe region on 14th July. It also shows the enlarged figure of the partial region in the study area. MODIS albedo is the comprehensive performance of the large pixel, so it is relatively smoother. Like MODIS albedo, the albedo acquired by two prior based methods can offer the same spatial character of the land surface, while they can offer more details of the surface. In the middle of enlarged map, we can see the narrow river, in the low left corner we can see that the result contains more information about topography and tectonic. The method Ⅰ uses a priori knowledge in the resolution of 500 m, so it will result in the mosaic phen-

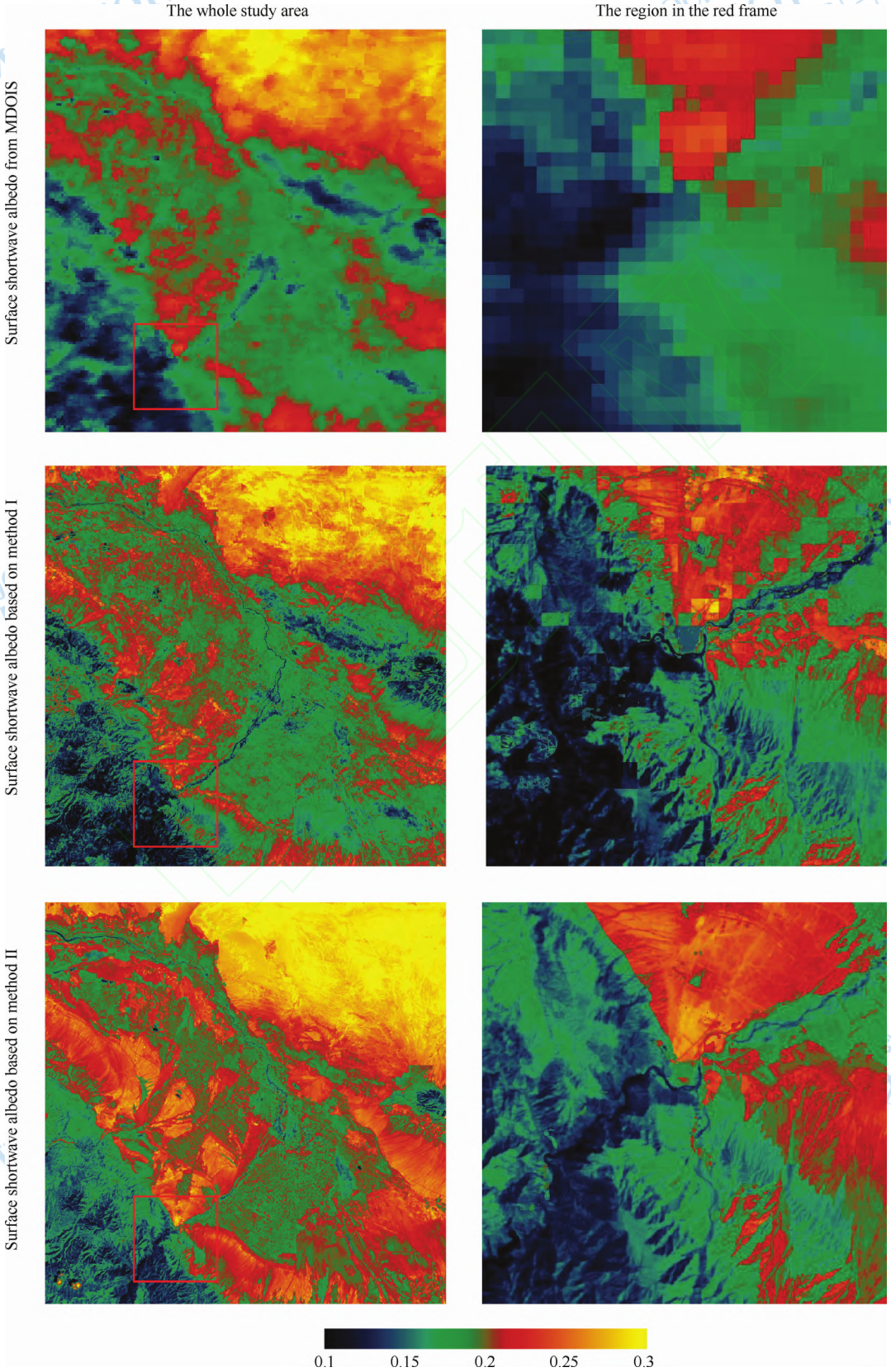

Fig.3 Maps of surface shortwave albedo of different methods on Aug 14th, 2009

omenon, especially in the Intersection region, while method Ⅱ performs better.

Fig.4 shows the mean and standard variance of albedo acquired by method I, Ⅱ, Ⅲ and MODIS production. In this study, we select four typical phenologies to study the influence of phenology in the inverse of albedo. In order to show the difference between results of various methods, we compared the statistics results of different land cover types with the MODIS albedo products. By comparing, inversion methods based on a priori knowledge have improved the albedo accuracy to varying degrees. Compared with MODIS albedos, the absolute and relative error of method Ⅲ is respectively 0.03 and 13%, while the method Ⅰ and Ⅱ are 0.01 and 4%. The improvement of the method Ⅰ and Ⅱ is independent with the land cover type. The relative error is mostly between 2% and 8%. The reason may be that the difference of BRDF shape between different classes and in the class is not obvious (Jiao, et al., 2011). So building a classification system of BRDF change will be helpful to the application of prior knowledge. The improvement by using a priori knowledge is dependent on the range of phenology. The improvement of the season with luxuriant vegetation is better than the fading time. For example, to the grassland, the relative error is 7% on April 4th while 1% on August 14th. Perhaps it is related with the different BRDF shape of vegetation in the growth period.

Some of the HJ-1 CCD data are influenced by the scattered cloud, which will influence the inverse of albedo for some land cover types. Method Ⅰ applies a pixel-to-pixel prior knowledge based method to calibrate the BRDF with only one-direction observation data, which will transmit all the error of the observation data to the calculation of albedo. The method Ⅱ uses the same prior knowledge for all the pixels, it balance the proportion of prior knowledge and observation information with the prior information ratio. It has some improvement in the error transmission of albedo inverse procedure.

According to the comparison and analyses above, we discovered that even though the method Ⅰ and method Ⅱ improve the inverse accuracy of the albedo compared with the method that assumes the ground is isotropic, the improvement of the accuracy is not obvious in the Heihe region. To analyze the reason, we choose one pixel from each four typical land cover types and draw the BRDF of four different phonologies in the red band and the corresponding reflectance at the same phenology and spatial position (Fig. 5). The position of the solar zenith and view zenith has a few changes as the phenology changes, which results in a relative change of the position in the BRDF. Sometimes the reflectance is near the hot spot region which owns a relative high reflectance such as the forest land in September in Fig. 5. If we take this reflectance to represent the reflectance under the isotropic assumption, the albedo will be higher compared with the traditional nadir observation. As we know, white sky albedo is the integral of BRDF. So the position of the observation may result in getting a relatively higher reflectance than the nadir view under the isotropic assumption for the data acquired by the HJ-1 CCD. Compared to method Ⅲ, the improvement of method Ⅰ is limited.

From Fig.5, we can also find that there is a high difference in the BRDF between different land cover types and so do in different phenologies. As the reflectance in April when the vegetation has not become green is mostly contributed by the bare land, the shape of BRDF appears to a typical roof shape. There is a typical peak value at the position of the hot spot. In May, the forest land and grassland begin to grow green while the crop has not been sown. So the reflectance of crop land and bare land is still appears a roof-shape BRDF while the forest land and grassland appears some characteristics of the bowl shape, which own a typical BRDF effect. All the land cover types except the bare land appear the bowl shape in August. The

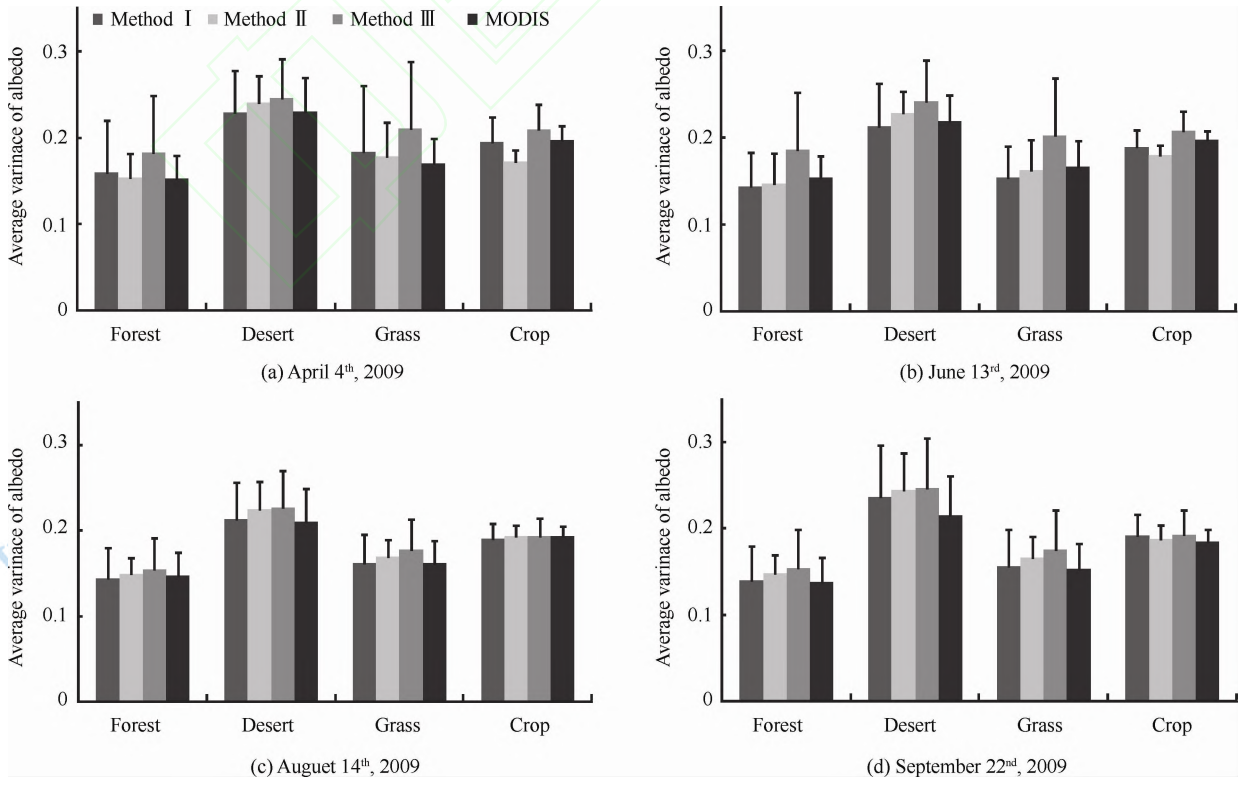

(a) April 4th, 2009 (b) June 13rd, 2009

(c) Auguet 14th, 2009 (d) September 22nd, 2009

Fig.4 Average and varinace of surface albedo obtained through the method I, method Ⅱ, method Ⅲ and MODIS at four land cover and four temporal (only shows the positive error bar)

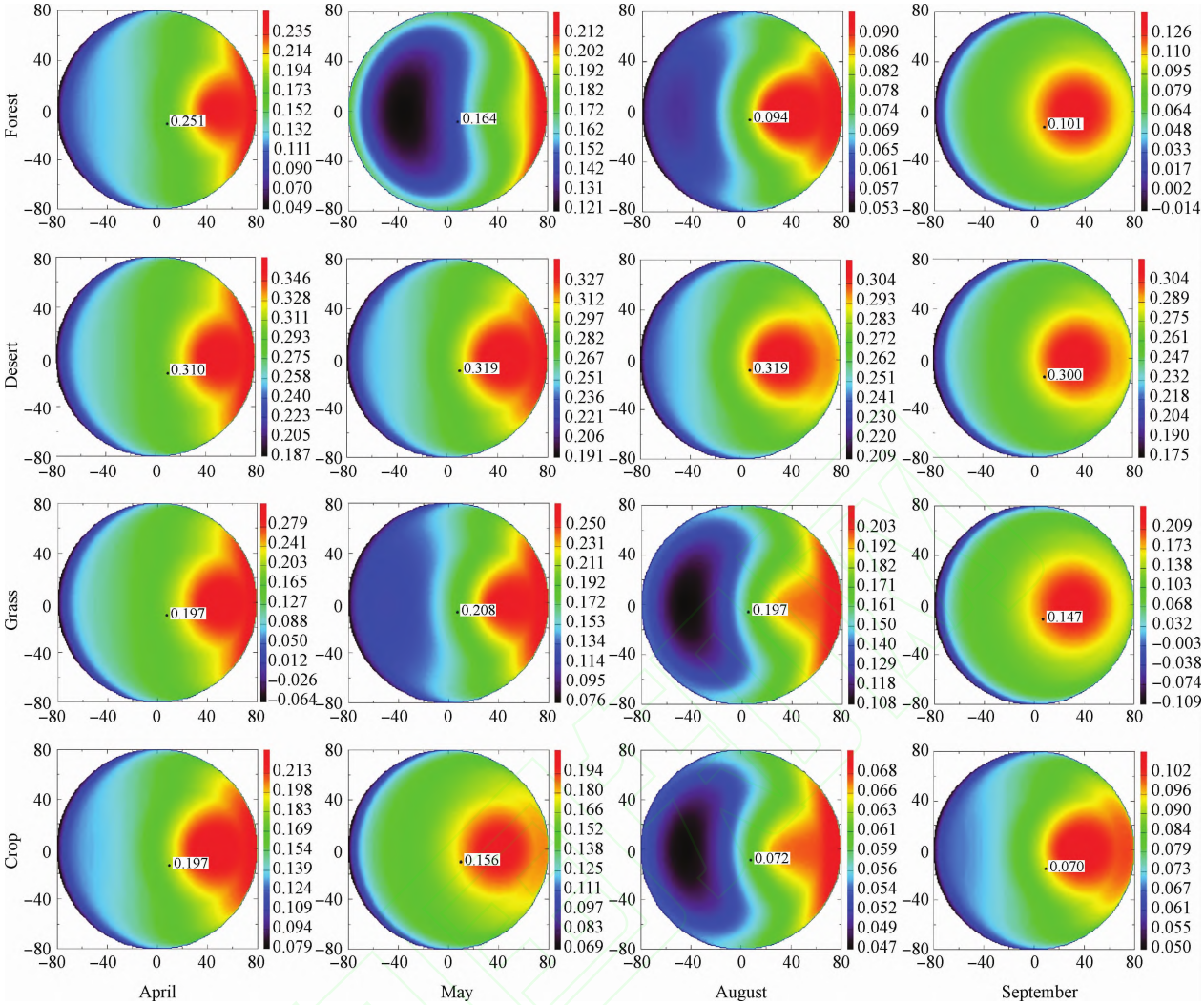

Fig.5 MODIS BRDF shape of four land covers in the red band at different temporal phases

(The BRDF shapes are showed in polar form, the center of the BRDF refer to the zenith direction, the distance to the center refers to the view or sun zenith angle, the polar angel represents the azimuth. Positive and negative values of the coordinates are used to distinguish the forward and backward of the observation. The dark point is the HJ-1 CCD observation)

shape of BRDF in September is similar with the shape in April except the crop land. The BRDF shape of bare land remains the same as the phenology changes. We can find a similar result through the near infrared band.

3.2 The validation by the ground observation data

The comparison of the remote sensing product with the ground observation data is an important procedure for the accuracy validation. To a certain extent, the ground observation data can represent the true state of land, but we could not acquire the ground data at the remote sensing scale. The underlying surface Yingke oasis station is relatively isotropic. The observation data is typical. To validate the accuracy of the result, we compare the ground data with the satellite data at different scales (Liang, et al., 2003). Fig. 6 shows the comparison of albedo acquired by three methods and the MODIS albedo with the ground observation data. Albedo changes significantly in different seasons. And it has the smallest value in summer due to the influence of chlorophyll. Method Ⅰ and Ⅱ together with MODIS products show a good uniformity with the ground observation data. Except for the day of 181 and 265, the absolute error between method Ⅰ and ground observation data ranges

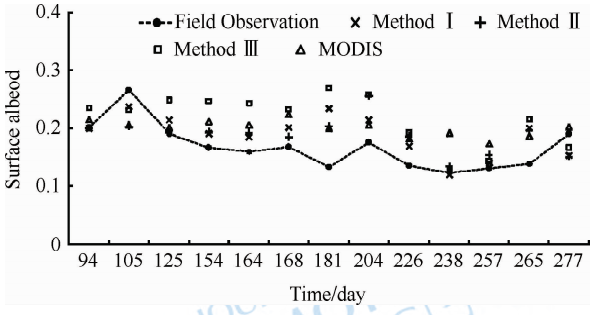

Fig.6 Time series of ground measurements albedo, MODIS albedo and HJ actual shortwave albedo obtained through the method Ⅰ, Ⅱ, Ⅲ at HJ satellite pass time over Yingke oasis station

from 0.02 to 0.05 and the average is 0.032, which meets the accuracy requirement of albedo application. There are 5, 4 and 8 days for method Ⅱ, Ⅲ and MODIS albedo that do not meet the accuracy requirement, the average absolute errors are 0.032, 0.057 and 0.042. At the same time we can see that the albedo of MODIS product is not sensitive to the change of season(Schaaf, 2002), which may be influenced by the mixture of pixels.

Fig.7 gives the scatter diagram of different methods and ground observation. The Root mean square errors (RMSEs) of the method I, method Ⅱ and MODIS product are 0.043, 0.046 and 0.048, respectively, and the relative error is around 20%. The RMSE of method Ⅲ based on the isotropic assumption is 0.069 and the relative error is as high as 36.3%. So the anisotropy should be taken into account in order to evaluate the albedo accurately.

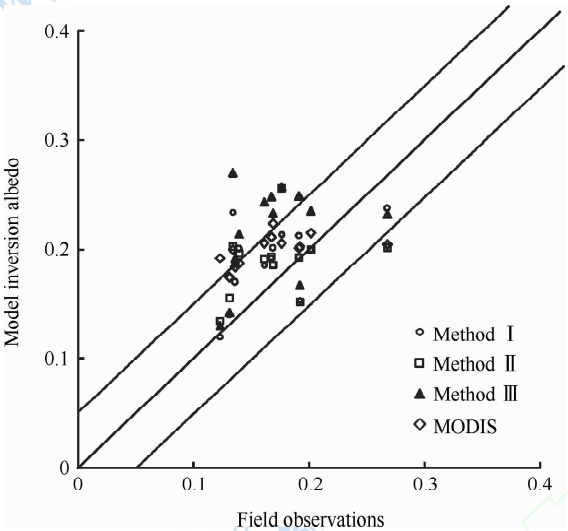

Fig.7 Scatter plot of surface albedo for the Yingke oasis station during HJ satellite pass time

Method Ⅰ and Ⅱ together with MODIS products show a good uniformity with the ground observation data in most cases, but sometimes there are still some differences. The reasons may be as below: (1) the scale effect of BRDF (Jin, et al., 2003). Method Ⅰ use the BRDF of the MODIS albedo product as the prior knowledge while there is an obvious scale effect between MODIS product and ground observation data. Method Ⅱ uses the limited ground observation data of all research regions in all phenologies without the consideration of the difference in phenology. (2) The influence by the accuracy of the HJ-1 CCD data. Method Ⅰ transmits all the error of the observation data to the calculation of albedo. Method Ⅱ balances the proportion of prior knowledge and observation information with the prior information ratio. The two methods are weak in defending the noise and need high quality observation data.

4 CONCLUSIONS AND DISCUSSIONS

A priori knowledge-based method can better improve inversion precision of surface albedo. This paper compared three algorithms based on retrieval of surface albedo using HJ data in Heihe experiment. The three algorithms include the backup algorithm of operational MODIS BRDF/Albedo product (method I), the Bayesian inference-based algorithm (method Ⅱ) and the assumption of a Lambertian surface reference algorithm (method Ⅲ). By comparing three results and MODIS product with surface observation data, results suggest several major conclusions:

In addition to capturing the majority of the ground texture, high resolution HJ surface albedo based on prior knowledge can also provide more surface details. However, method Ⅰ used the same BRDF shape as the prior knowledge in a 500 m MODIS pixel, and the results showed mosaic appearance which is particularly significant in fracture area. Compared to method Ⅰ, method Ⅱ showed relatively uniform result.

In lacking of space-borne multi-angular observation data, introducing the prior knowledge of surface anisotropy can effectively improve inversion precision of surface albedo. According to different surface types statistics, compared to MODIS albedo product, absolute error of the assumption of a Lambertian surface reference algorithm is 0.03, and the relative error is 13%. The method based on prior knowledge has the absolute error of 0.01 and relative error of 4%.

For HJ data, in statistical sense, method Ⅰ and method Ⅱ are similar in improving surface albedo inversion precision compared to MODIS albedo product. Method Ⅱ only used limited surface observation data as prior knowledge for all the data, and adjusted the proportion of prior knowledge in the results through priori information ratio. Method Ⅰ which used MODIS BRDF shape of the same time phase as the prior knowledge is a pixel to pixel application. Compared to surface observation data, the absolute error of method Ⅰ and method Ⅱ are less than 0.05, and relative error are less than 23%, while the results of method Ⅲ are 0.069 and 36.3%, respectively. This is generally in line with early results of Kimes (1985).

The improvement of different methods for albedo almost does not depend on surface types, and has the relative error between 2%—8%. However, the dependence of the phase change is more significant. The improvement on green-up season is significantly stronger than dormancy season which is probably related to vegetation anisotropic characteristics during the growing process.

For single observation angle, the major restriction of the backup algorithm of operational MODIS BRDF/Albedo product relies on hard adjustment of priori BRDF shape, so the result is mainly influenced by single error. If adopting more than two observations, the method can be more effective. Now the idea has been adopted in albedo operational backup algorithm since from the MODIS five product.

The above two prior knowledge-based albedo methods may somewhat depend on sensor specifications, region location, surface type and time phase. Because different sensor specifications will decide the relative position of the sun and observation geometry, and then effect the adjustment of priori BRDF shape. The changes of region location and time phase affect the geometry of the sun. Meanwhile, the BRDF shape changes of different surface types need further study. Finding and applying a classification system based on BRDF shape as well as building typical surface type BRDF prior knowledge database for making effectively use of BRDF prior knowledge are the highlight of our work in future.

Acknowledgements: Many thanks to Yang Hua, the professor of Geography of school in Beijing Normal University, Many thanks also to China centre for resources satellite data and application, environment and ecological Science data Center for west China.

REFERENCES

Deering D and Leone P. 1986. A sphere-scanning radiometer for rapid directional measurements of sky and ground radiance. Remote Sensing of Environ, 19(1): 1-24 [DOI: 10.1016/0034-4257(86)90038-6]

Dickinson R E. 1995. Land processes in climate models. Remote Sensing of Environment, 51(1): 27-38 [DOI: 10.1016/0034-4257 (94) 00062-R]

Du X, Chen X Y, Meng J H, Zhang F F, Zhang M and Wu B F. 2010.

Atmospheric correction of HJ-1 CCD data based on 6S model. Remote Sensing for Land and Resources, 21(2): 22-25

Eidenshink J C and Faundeed J L. 1994. The 1-km AVHRR global land data set: first stages in implementation. International Journal of Remote Sensing, 15(17): 3443-3462 [DOI: 10.1080/01431169408954339]

Hu B X, Lucht W G, Li X W and Strahler A H. 1997. Validation of kernel-driven semiempirical models for the surface bidirectional reflectance distribution function of land surfaces. Remote Sensing of Environment, 62(3): 201-214 [DOI: 10.1016/S0034-4257(97)00082-5]

Irons J R, Campbell G S, Norman J M, Graham D W and Kovalick W M. 1992. Prediction and measurement of soil bidirectional reflectance. IEEE Transactions on Geoscience and Remote Sensing, 30(2): 249-260 [DOI: 10.1109/36.134075]

Jiao Z T, Li X W, Wang J D and Zhang H. 2011. Assessment of MODIS BRDF shape indicators. Journal of Remote Sensing, 15(3): 432-456

Jin Y F, Schaaf C B, Gao F, Li X W, Strahler A H, Lucht W and Liang S L. 2003. Consistency of MODIS surface bidirectional reflectance distribution function and Albedo retrieval: 1. Algorithm Performance. Journal of Geophysical Research, 108(D5): 4158 [DOI: 10.1029/2002JD002803]

Kimes D S and Seller P J. 1985. Inferring hemispherical reflectance of the Earth's surface for global energy budgets from remotely-sensed nadir or directional radiance values. Remote Sensing Environment, 18(3): 205-223 [DOI: 10.1016/0034-4257(85)90058-6]

Kimes D S, Newcomb W W, Nelson R F and Schutt J B. 1986. Directional reflectance distributions of a hardwood and pine forest canopy. IEEE Transactions on Geoscience and Remote Sensing, 24(2): 281-293 [DOI: 10.1109/TGRS.1986.289647]

Leroy M and Breon F M. 1996. Surface reflectance angular signatures from airborne POLDER data. Remote Sensing Environment, 57: 97-107

Lewis P and Barnsley M J. 1994. Influence of the sky radiance distribution on various formulations of the earth surface albedo. Proceedings of Conference on Physical Measurements of Signatures in Remote Sensing, Courchevel, France. International Society for Photogrammetry and Remote Sensing: 707-715

Li X W, Gao F, Wang J D and Strahler A H. 2001. A priori knowledge accumulation and its application to linear BRDF model inversion. Journal of Geophysics Research, 106(D11): 11925-11935 [DOI: 10.1029/2000JD900639]

Li X W, Wang J D, Hu B X and Strahler A H. 1998. Application of Priori knowledge in remote sensing inversion. Science China (Series D), 28(1): 67-72

Liang S L. 2001. Narrowband to broadband conversions of land surface albedo: I. algorithms. Remote Sensing of Environment, 76(2): 213-238 [DOI: 10.1016/S0034-4257(00)00205-4]

Liang S L, Fang H L, Chen M Z, Shuey C J, Walthall C, Daughtry C, Morisette J, Schaaf C and Strahler A. 2002. Validating MODIS land surface reflectance and albedo products: methods and preliminary results. Remote Sensing of Environment, 83(1/2): 149-162 [DOI: 10.1016/S0034-4257(02)00092-5]

Liang S L, Shuey C J, Russ A L, Fang H L, Chen M Z, Walthall C L, Daughtry C S T and Hunt R. 2003. Narrowband to broadband conversions of land surface albedo: II. Validation. Remote Sensing of Environment, 84(1): 25-41 [DOI: 10.1016/S0034-4257(02)00068-8]

Liu J C, Schaaf C, Strahler A, Jiao Z, Shuai Y M, Zhang Q L, Roman M, Augustine J A and Dutton E G. 2009. Validationof moderate resolution imaging spectroradiometer (MODIS) albedo retrieval algorithm: dependence of albedo on solar zenith angle. Journal of Geophysical Research, 114(D1): D01106 [DOI: 10.1029/2008JD009969]

Lucht W, Schaaf C B and Strahler A H. 2000. An algorithm for the retrieval of albedo from space using semiempirical BRDF models. IEEE Transactions on Geoscience and Remote Sensing, 38(2): 977-998 [DOI: 10.1109/36.841980]

Ma M G, Wang W Z, Huang G H, Zhang Z H and Tan J L. 2008. WATER: Dataset of automatic meteorological observations at the Yingke oasis station. Cold and Arid Regions Environmental and Engineering Research Institute. Chinese Academy of Sciences

Nicodemus F E, Richmond J C, Hsia J J, Ginsberg W I and Limperis T. 1977. Geometrical Considerations and Nomenclature for Reflectance. Washington, DC: Institute for Basic Standards, NBS MN-160

Pokrovsky O and Roujean J L. 2002. Land surface albedo retrieval via kernel-based BRDF modeling: statistical inversion method and model comparison. Remote Sensing Environment, 84(1): 100-119 [DOI: 10.1016/S0034-4257(02)00100-1]

Ranson K J, Biehl L L and Bauer M E. 1985. Variation in spectral response of soybeans with respect to illumination, view and canopy geometry. International Journal of Remote Sensing, 6(12): 1827-1842 [DOI: 10.1080/01431168508948331]

Rodgers C D. 1976. Retrieval of atmospheric temperature and composition from remote measurements of thermal radiation. Reviews of Geophysics, 14(4): 609-624 [DOI: 10.1029/RG014i004p00609]

Roujean J L, Leroy M and Deschamps P Y. 1992. A bidirectional reflectance model of the earth's surface for the correction of remote sensing data. Journal of Geophysical Research, 97(D18): 20455-20468 [DOI: 10.1029/92JD01411]

Salomon J G, Schaaf C B, Strahler A H, Gao F and Jin Y F. 2006. Validation of the MODIS bidirectional reflectance distribution function and albedo retrievals using combined observations from the aqua and terra platforms. IEEE Transactions on Geoscience and Remote Sensing, 44(6): 1555-1565 [DOI: 10.1109/TGRS.2006.871564]

Schaaf C B, Gao F, Strahler A H, Lucht W, Li X W, Tsang T, Strugnell N C, Zhang X Y, Jin Y Y, Muller J P, Lewis P, Barnsley M, Hobson P, Disney M, Roberts G, Dunderdale M, Doll C, d'Entremont R P, Hu B X, Liang S L, Privette J L and Roy D. 2002. First operational BRDF, Albedo Nadir reflectance products from MODIS. Remote Sensing of Environment, 83(1/2): 135-148 [DOI: 10.1016/S0034-4257(02)00091-3]

Schaaf C L B, Liu J, Gao F and Strahler A H. 2011. MODIS albedo and reflectance anisotropy products from Aqua and Terra, land remote sensing and global environmental change // Ramachandran B, Justice C, Abrams M, eds. NASA's Earth Observing System and the Science of ASTER and MODIS, Remote Sensing and Digital Image Processing Series, Vol. 11. New York: Springer-Cerlag: 873 [DOI: 10.1016/j.rse.2011.04.019]

Shuai Y M, Masek J G, Gao F and Schaaf C B. 2011. An algorithm for the retrieval of 30-m snow-free albedo from Landsat surface reflectance and MODIS BRDF. Remote Sensing of Environment, 115(9): 2204-2216 [DOI: 10.1016/j.rse.2011.04.019]

Strugnell N and Lucht W. 2001. An algorithm to infer continental-scale albedo from AVHRR data, land cover class and field observations of typical BRDF's. Journal of Climate, 14: 1360-1376

Strugnell N C, Lucht W and Schaaf C. 2001. A global albedo data set derived from AVHRR data for use in climate simulations. Geophysical Research Letters, 28(1): 191-194 [DOI: 10.1029/2000GL011580]

Sun Y, Gu X F and Yu T. 2010. A study of HJ-1A CCD image atmospheric correction. Remote Sensing for Land and Resources, 87(4): 6-9

Tarantola A. 1987. Inverse Problem Theory: Methods for Data Fitting and Model Parameter Estimation. New York: Elsevier Science: 613

Tsay S C, King M D, Arnold G T and Li J Y. 1998. Airborne spectral measurements of surface anisotropy during SCAR-B, Journal of Geophysical Research, 103(D24): 31943-31953 [DOI: 10.1029/98JD01167]

Wang Y F, Li X W, Nashed Z, Zhao F, Yang H, Guan Y N and Zhang H. 2007. Regularized kernel based BRDF model inversion method for ill-posed land surface parameter retrieval. Remote Sensing of Environment, 111(1): 36-50 [DOI: 10.1016/j.rse.2007.03.007]

Wang J D, Zhang L X, Liu Q H, Zhang B and Yin Q. 2009. The spectrum database of typical objects in China. Beijing: Science Press: 231-290

Wanner W, Li X W and Strahler A H. 1995. On the derivation of kernels for kernel-driven models of bidirectional reflectance. Journal of Geophysical Research, 100(D10): 21077-21090 [DOI: 10.1029/95JD02371]

Yang H, Xu W L, Zhao H R, Chen X and Wang J D. 2003. Information stream and its control in the inversion of Quantitative remote sensing regularization of inversion. Science in China (Series D), 33(8): 799-808

先验知识估算 HJ-1 CCD 数据地表反照率

张虎, 焦子锑, 李小文, 黄兴英, 董亚冬

1. 北京师范大学 地理学与遥感科学学院, 北京 100875;
2. 遥感科学国家重点实验室 北京师范大学, 北京 100875;
3. 数字城市北京市重点实验室, 北京 100875

摘 要:以黑河实验区为例,基于 HJ-1 CCD 数据和中分辨率成像光谱仪(MODIS) 二向性反射(BRDF)和反照率产品的备用算法(算法Ⅰ),贝叶斯原理的反照率反演算法(算法Ⅱ)和地表朗伯假设的算法(算法Ⅲ)成功估算了地表短波反照率。对反演结果进行分析并与地表观测数据进行比较,结果表明: (1) 高分辨率的 HJ-1 卫星地表反照率不仅能够提供下垫面主要的空间分布特征,还能提供地表细部结构;(2) 两种基于先验知识的地表反照率和 MODIS 产品接近,绝对误差为 0.01,相对误差为 4%,而算法Ⅲ的绝对误差为 0.03,相对误差为 13%; 算法Ⅰ和Ⅱ对反照率的改善对地表类型的依赖不明显,相对误差集中在 2%—8%,反演结果对时相变化依赖较为显著,在植被最茂盛的季节反照率改善作用明显优于凋谢季。(3) 算法Ⅰ和算法Ⅱ的结果与地表观测结果更为吻合,均方根误差在 0.05 以内,相对误差小于 23%,而算法Ⅲ的均方根误差为 0.069,相对误差为 36.3%;(4) 先验知识的作用可能依赖于太阳和观测几何的相对位置,因此可能依赖于季节和纬度的变化,以及传感器的成像方式。该研究对缺乏多角度观测的星载传感器的反照率反演有重要的参考价值。

关键词:HJ-1 CCD,MODIS,BRDF,反照率,贝叶斯推论,先验知识

中图分类号:TP701 **文献标志码**:A

引用格式:张虎,焦子锑,李小文,黄兴英,董亚冬. 2013. 先验知识估算 HJ-1 CCD 数据地表反照率. 遥感学报,17(2): 286-307

Zhang H, Jiao Z T, Li X W, Huang X Y and Dong Y D. 2013. A priori knowledge application in the retrieval of surface albedo using HJ-1 CCD data. Journal of Remote Sensing, 17(2): 286-307

1 引 言

地表反照率是广泛应用于地表能量平衡、中长期天气预报和全球变化研究的重要参数之一,对于全球和区域气候模型研究具有重要意义(Dickinson, 1995)。它定义为地表各个方向反射的全部光通量与总入射光通量的比值。地表的各向异性反射特性通常用 BRDF 来描述,BRDF 定义为来自光照方向地表辐照度的微增量与其引起的观测方向上反射辐射亮度增量的比值(Nicodemus 等,1977)。不同地表类型的 BRDF 可能存在差异(Strugnell 和 Lucht,2001; Jin 等,2003),精确估算地表反照率,需要考虑地表各向异性反射的影响。

遥感数据具有提供区域和全球分布的优势,但通常情况下获取的多角度观测数据依然有限。目前,在缺乏多角度观测的情况下,应用单一方向观测的遥感数据估算地表反照率通常有 3 种算法:

算法Ⅰ是目前 MODIS BRDF/反照率业务化运行的备用算法(Strugnell 等,2001)。早期基于甚高分辨率辐射计(AVHRR)的研究结果表明,该算法利用地表各向异性的反射特点,可以较好改善由于观测角度不足所带来的地表反照率估算精度低的问题(Strugnell 和 Lucht,2001; Strugnell 等,2001)。目前,该算法使用的 BRDF 原型库,已升级为像元-像元的 BRDF 数据库(Schaaf 等,2002)。通过地表通量塔观测的反照率验证表明,基于这些 BRDF 数据库和备用算法估算的 MODIS 地表“量反演”(magnitude inversion)的结果,和基于 MODIS“全反演”(full

收稿日期:2011-08-01;**修订日期**:2012-06-14

基金项目:国家自然科学基金(编号:40871193);遥感科学国家重点实验室自由探索项目(编号:610ZY-06);国家科技支撑项目(编号:2008BAC34B03)

第一作者简介:张虎(1986—),男,硕士,研究方向为定量遥感、地表二向性反射以及地表反照率的应用研究。E-mail: askzhanghu@126.com

通信作者简介:焦子锑(1970—),男,博士,副教授,主要研究领域包括定量遥感、地表各向异性反射的建模与应用,以及多角度信号用于地表分类的研究。已发表论文 20 余篇。E-mail: jiaozt@bnu.edu.cn

inversion)的反照率结果的差别很小(Jin 等,2003; Salomon 等,2006; Liu 等,2009)。

算法Ⅱ是基于贝叶斯原理,应用地表 BRDF 先验知识的反照率反演算法(Li 等,2001)。其基本思想是基于地表观测数据的模型参数的先验估计值及其协方差矩阵作为先验知识,通过最大似然法最小化代价函数得到贝叶斯最大似然解。该算法适用于传感器 BRDF 采样能力差、采样能力不足的数据,克服了像元-像元 BRDF 数据库数据量大的缺点,为全球 BRDF 知识库的建立,以及全球 BRDF 和反照率的反演提供了一个新的理论框架。其主要问题可能是 BRDF 先验知识的积累,以及建立约束 BRDF 先验知识(硬边界,δ 边界和软边界)的简单有效的指标。

算法Ⅲ直接假设地表为朗伯表面,用传感器的单方向观测数据代替地表反照率,这种算法未考虑地表各向异性反射的影响,不符合科学界几十年来对地球表面各向异性反射研究的事实,Kimes(1985)应用早期地面观测的研究结果表明,基于地面朗伯假设所估算的地表反照率可引起高达 45% 的误差。

先验知识是解决反演中信息量不足问题的关键。遥感信号信息量总是有限的,因此基于地面目标先验知识的积累和应用,对于提高地表参数的反演精度具有重要作用(Li 等,2001)。先验知识在地表反照率反演中的作用也逐渐受到重视,李小文等人(1998)阐述了先验知识在遥感反演中的重要作用,并基于一个核驱动 BRDF 模型,对地表观测的不同分辨率 BRDF 数据进行拟合,获取模型参数作为地表 BRDF 的先验知识库(Li 等,2001); Pokrovsky 等人(2002)应用统计的方法反演 BRDF 模型; MODIS BRDF 和反照率产品的备用算法基于地表先验 BRDF 数据库(Strugnell 和 Lucht,2001); Wang (2007)考虑了反演的正则化策略,提出了当观测严重不足或观测方向范围有限,或者是观测数据高度线性相关以及噪声的污染时,地表参数反演的正则化方法。

本文主要目标是通过应用业务化运行的半经验核驱动 BRDF 模型(RossThick-LiSparse-Reciprocal: RTLSR)(Lucht 等,2000)和 HJ-1 卫星 30 m 分辨率 CCD 数据,基于 MODIS BRDF/反照率产品的备用算法(算法Ⅰ)和贝叶斯原理的反照率反演算法(算法Ⅱ)反演地表反照率,并将初步反演结果和朗伯假设反照率(算法Ⅲ)以及 MODIS 反照率产品进行对比分析,最后与地表实测数据进行比较,分析和评价不同算法反演反照率的差异,为研究新算法和生产区域高分辨率的反照率产品提供算法基础。

1.1 研究区概况

研究区位于黑河流域的中上游,河西走廊的中段,主要包括张掖市、周边绿洲区以及祁连山的一部分,区域内山区、平原绿洲区和荒漠区具有截然不同的自然景观,地表覆盖季节差异大,对研究地表反照率具有较好的代表性。研究区的海拔约为 1500 m,其中林地、草地、农田和裸地 4 种地表类型占总面积的 95%。研究区范围内设有盈科灌区绿洲地表通量塔观测站,其下垫面主要地表类型为农田(玉米和小麦),能够获得宽波段(305—2800 nm)的反照率数据(马明国 等,2008)。

1.2 数据介绍与处理

本研究中用到的数据包括 HJ-1 CCD 数据、MODIS 产品(反照率数据 MCD43、气溶胶数据 MOD04、物候数据 MCD12Q2)、地表 73 组实测数据(Hu 等,1997; Strugnell 等,2001; Li 等,2001),地表气象站观测数据以及研究区地表类型图等。

HJ-1 CCD 数据由环境与灾害监测预报小卫星星座 A、B 星获得,两颗卫星的 4 台 CCD 相机谱段设置和空间分辨率相同。星下点对称放置,平分视场、并行观测、联合完成,传感器对地刈幅(swath)宽度为 700 km,地面像元分辨率为 30 m,两台 CCD 相机组网后重访周期为 2 d。不同于传统美国陆地卫星 TM 传感器的天顶观测方式,HJ-1 CCD 相机提供最大观测天顶角在 35°左右。图 1 以极坐标的形式给出了 6 月份研究区内某一像元的太阳和观测几何的空间分布图。从图中可以看出,在 6 月份,HJ-1 A 和 B 两颗卫星提供了近 14 个方向的观测,这些观测分布在垂直主平面附近,在一定程度上反映了地表各向异性反射。图 1 是联合了 A,B 两颗卫星,在没有考虑数据质量的情况下得出的,在实际的应用中,由于受到云的影响,很难将这些观测全部应用于研究。对研究区的 CCD 数据基于 6S 方法进行了进一步的大气校正,初步验证结果表明,经 6S 大气校正后的 CCD 数据在草地和裸土的平均误差在红波段约为 8%,在近红外波段平均误差为 35%(孙源等,2010),冬小麦在近红外波段的平均误差为 3%(杜鑫 等,2010)。考虑到研究区范围不大,且文中选

定的数据大气能见度高,气溶胶光学厚度小,在本研究区中,气溶胶光学厚度取 MODIS 气溶胶产品(MOD04)在研究区范围的均值。通过比较不同类型校正前后地物光谱曲线(王锦地 等,2009)和归一化植被指数(NDVI),结果表明该方法较好地消除了大气的影响作用,我们所用实验区的大气校正的误差应小于 10%。研究区地表类型数据是通过综合 2009 年 5 月 22 日的 HJ-1B CCD2 数据和土地利用图得出。

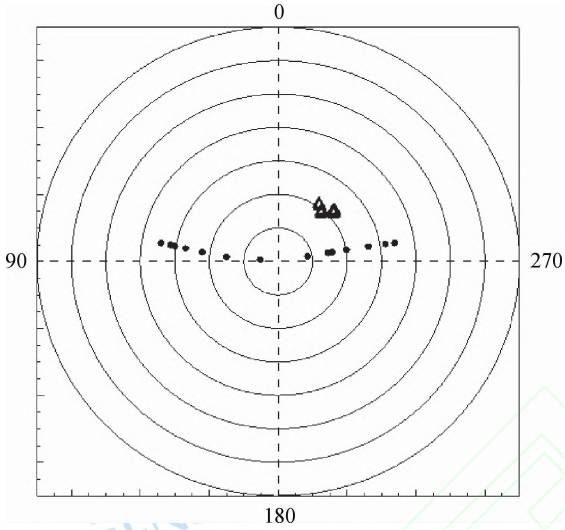

图 1 2009 年 6 月份 HJ-1 CCD 观测几何采样空间分布图(圆的半径代表天顶角,间隔为 10°,圆心处代表天顶角方向为 0 度,极坐标表示方位角,沿顺时针方向增大,黑点表示观测位置,三角形表示太阳的位置)

MODIS 是美国对地观测系统中的重要传感器,其算法中使用的是经过大气校正的多天、多波段的反射率数据,提供以 16 d 为周期的全球反照率和 BRDF 产品(Schaaf 等,2002,2011)。对 MODIS 反照率产品的比较验证,目前已积累了大量的工作(Liang 等,2002; Jin 等,2003; Salomon 等,2006; Liu 等,2009),结果表明宽波段的反照率绝对精度可达到 0.02—0.05,对非冰雪类型质量更为可靠。其反照率产品在全球范围内应用较为广泛,是国际遥感界较为认可的产品之一,目前估算单一角度高分辨率反照率通常也采用 MODIS 反照率产品作为先验知识(Shuai 等,2011)。同样在算法 Ⅰ 中,我们也将 MODIS 反照率产品作为下垫面 BRDF 的先验知识,根据研究区经纬度信息,用 MODIS 重投影工具(MRT)裁减出研究区,将 MODIS 反照率产品采用最邻近像元法重采样到 30 m 分辨率。HJ-1 CCD 和 MODIS 波段特征如表 1 所示。

表 1 MODIS 和 HJ-1 CCD 传感器特征

传感器		MODIS		HJ-1 CCD	
空间分辨率		500 m		30 m	
光谱范围	波段名称	波段号	间隔/nm	波段号	间隔/nm
	蓝	3	459—479	1	430—520
	绿	4	545—565	2	520—600
	红	1	620—670	3	630—690
	近红外	2	841—846	4	760—900

地表实测的 73 组数据主要为算法 Ⅱ 提供先验知识,它包括多种地表类型的多角度数据,大部分的数据来源于 FIFE 和 BOREAS 地面实验,这部分数据的传感器类型为 PARABOLA (Deering 等,1986);还有一部分数据来源于 Kimes 等人(1985,1986),Ranson 等人(1985)和 Irons 等人(1992),其余的数据还包括 AVHRR 数据(Eidenshink 等,1994),机载的地球极化与方向反射测量仪(POLDER)数据(Leroy 等,1996)和 SCAR 数据(Tsay 等,1998)。这些数据只包含红和近红外两个波段,大部分数据曾被用来验证半经验的核驱动模型的拟合能力以及进行算法的研究(Li 等,2001; Hu 等,1997),这些数据具有很好的代表性。首先选用核驱动模型(RTLSR)对数据进行拟合,并根据拟合数据和观测数据的差异,选择合适的阈值,对观测噪声较大的点进行平滑(Li 等,2001),剔除了拟合误差大或包含雪或水体的数据,最终选择其中 69 组数据参与计算。

盈科灌区绿洲站自动气象站位于甘肃省张掖市的盈科灌区农田内,观测点的地理坐标为(100°25′E,38°51′N),海拔高度为 1519 m,仪器架高为 2.81 m,连续观测和记录 305—2800 nm 半球空间内的上行辐射和下行辐射能量,经处理后的数据每隔 10 min 有一个观测值(马明国 等,2008)。该数据主要用于对比各算法反演反照率的结果,在比较过程中我们采用 HJ-1 卫星过境前后 20 min 地表观测数据的均值。

2 基于先验知识的反照率算法

本节首先概述了半经验的核驱动 BRDF 模型,然后简要介绍了 MODIS 业务化运行反照率反演的备用算法(算法 Ⅰ)和基于贝叶斯推论的反照率反演算法(算法 Ⅱ),最后概括了不同算法间反照率反演结果的比较方法。

核驱动模型用有一定物理意义的核的线性组合来描述地表的二向性反射特征,即对于地表的一

个非朗伯像元，其表面散射可以表示为各向同性散射，体散射和几何光学散射不同散射组分的加权和的形式(Roujean 等，1992; Wanner 等，1995; Lucht 等，2000):

$$R(\theta_i,\theta_r,\varphi)=f_{iso}(\lambda)+f_{vol}(\lambda)K_{vol}(\theta_i,\theta_r,\varphi)+f_{geo}(\lambda)K_{geo}(\theta_i,\theta_r,\varphi) \quad (1)$$

式中，R 为二向性反射，K_{vol} 为体散射核，描述水平均匀植被的各向异性散射；K_{geo} 为几何光学核，描述从观测方向上地物 3 维结构及其相互投射阴影等作用产生的几何光学散射，它们都是入射角和观测角的函数；θ_i，θ_r 和 φ 分别表示光线入射天顶角和观测天顶角及相对方位角；f_{iso}，f_{geo} 和 f_{vol} 分别表示各向均匀散射、体散射和几何光学散射这 3 部分在二向性反射中所占的比例，它们是波长的函数。因为核是与待反演参数无关、只与太阳天顶角有关的函数，核的积分可以预先求出，将核的积分以 f_{iso}，f_{vol} 和 f_{geo} 为权重相加，就得到相应的黑天空反照率(ρ_{bs})和白天空反照率(ρ_{ws}) (Nicodemus 等，1977; Lucht 等，2000)。这两种反照率的组合却能在很大程度上描述地表真实反照率，即真实地表反照率(Lewis 和 Barnsley，1994):

$$\alpha(\theta_i)\approx[1-S(\tau)]\rho_{bs}(\theta_i)+S(\tau)\rho_{ws} \quad (2)$$

式中，$S(\tau)$ 是天空散射光所占的比例，它是光学厚度 τ 的函数，除在非常大的太阳天顶角情况下，式(2)都能够很好地近似得到地表真实反照率。

2.1 算法Ⅰ-基于 MODIS 反照率备用算法

算法Ⅰ的基本原理是假设相同地表类型的 BRDF 形状相似并可提前预测，通过观测数据拟合先验 BRDF 形状得到反照率(Strugnell 等，2001; Jin 等，2003)。在该算法中，我们引入了 MODIS 的 RTLSR 模型参数产品(MCD43A1)，作为下垫面各向异性反射模式的先验知识。模型参数空间提供的下垫面 BRDF 参数，经过前向模拟，可以计算出给定太阳几何的 BRDF 原型，当传感器提供少数几个多角度观测时，通过最小二乘法，对预先给定的 BRDF 形状进行拟合，得到拟合观测数据最优的 BRDF 形状位置，进而得到地表反照率。很明显，对于 HJ-1 CCD 传感器，当只有一个角度观测数据时，数据对先验 BRDF 形状的拟合误差为零，表示预先定义的 BRDF 先验形状完全通过该观测点。对于同一地物，MODIS 和 HJ-1 CCD 数据的 BRDF 形状将非常相似，并不会出现截然不同的情况，因此可以将二者的关系表示为 $BRDF_{hj}=a\times BRDF_m$，其中 $BRDF_m$ 表示先验 MODIS BRDF 形状，该先验的 BRDF 形状从整体上刻画了对应的 HJ-1 像元的 BRDF 特征，$BRDF_{hj}$ 表示通过 MODIS BRDF 得到的相应 HJ-1 BRDF 形状，a 是一个乘数因子，用于从 MODIS BRDF 拟合出与其相似的 BRDF 形状，可通过方向反射率的关系得到，公式表示为：$a=\rho_o/\rho_s$，其中 ρ_o 为 CCD 观测数据，ρ_s 是对模型参数通过核驱动模型前向计算得出的与 CCD 数据有相同入射和出射几何的反射率。需要说明的是，在此算法中虽然将 MODIS 的 BRDF 作为下垫面各向异性先验知识，但其仅提供了下垫面 BRDF 形状，用于提高反照率的反演精度，地表反照率的大小取决于 HJ-1 CCD 数据。

2.2 算法Ⅱ-基于贝叶斯推论

算法Ⅱ是基于贝叶斯推论反演 HJ-1 CCD 地表反照率算法。当观测数目不足或 BRDF 空间采样不足，反演结果将变得不稳定，贝叶斯推论通过先验知识的积累和应用，是解决反演不确定问题的有效方法。该算法把 BRDF 模型参数看成是具有某种先验分布的随机变量，结合样本数据，通过最大似然估计，推断参数的后验分布(Li 等，2001)。在此算法中，先验知识并不针对某一种地表类型，不同地物的差异主要是通过观测数据来体现，通过观测数据对先验知识对进行调整，从而反演地表反照率。在实际应用过程中，可通过最小化代价函数来得到贝叶斯最大似然解(Rodgers，1976; Tarantola，1987):

$$\mathrm{Cost}(\boldsymbol{X})=(\boldsymbol{A}_{obs}\boldsymbol{X}-\boldsymbol{Y}_{obs})^{\mathrm{T}}\boldsymbol{C}_d^{-1}(\boldsymbol{A}_{obs}\boldsymbol{X}-\boldsymbol{Y}_{obs})+(\boldsymbol{X}-\boldsymbol{X}_0)^{\mathrm{T}}\boldsymbol{C}_p^{-1}(\boldsymbol{X}-\boldsymbol{X}_0) \quad (3)$$

$\boldsymbol{A}_{obs}$ 为核矩阵，$\boldsymbol{Y}_{obs}$ 为实测的反射率数据，$\boldsymbol{C}_d$ 为观测误差的协方差，$\boldsymbol{C}_p$ 是模型先验参数的 $\boldsymbol{X}_{obs}$ 协方差矩阵，$\boldsymbol{X}_0$ 为先验知识对模型参数 $\boldsymbol{X}$ 的一个最优估计，取观测数据总体得到的参数的平均值，表 2 中列出了由 69 组数据归纳的模型参数的先验分布。代价函数式(3)由两部分构成，一部分是数据拟合误差，另一部分是方向观测和先验知识相应方向模拟值的偏离。在不能够得到观测误差协方差矩阵的情况下，通过在观测项加上一个权重项，以衡量观测信息在反演结果中占的比重，代价函数可以改写为(Li 等，2001):

$$\mathrm{Cost}(\boldsymbol{X})=n(\boldsymbol{A}_{obs}\boldsymbol{X}-\boldsymbol{Y}_{obs})^{\mathrm{T}}(\boldsymbol{A}_{obs}\boldsymbol{X}-\boldsymbol{Y}_{obs})+(\boldsymbol{X}-\overline{\boldsymbol{X}})^{\mathrm{T}}\boldsymbol{A}_{simu}^{\mathrm{T}}\boldsymbol{A}_{simu}(\boldsymbol{X}-\boldsymbol{X}_0) \quad (4)$$

其最小二乘解为(杨华 等，2003):

$$\boldsymbol{X}=(n^2\boldsymbol{A}_{\text{obs}}^{\text{T}}\boldsymbol{A}_{\text{obs}}+\boldsymbol{C}_{\text{p}}^{-1})^{-1}\begin{bmatrix}n\boldsymbol{A}_{\text{obs}}\\ \boldsymbol{A}_{\text{simu}}\end{bmatrix}\begin{bmatrix}n\boldsymbol{y}_{\text{obs}}\\ \boldsymbol{Y}_{\text{simu}}\end{bmatrix} \quad (5)$$

式中,$\boldsymbol{\Lambda}$ 和 $\boldsymbol{E}$ 分别是模型参数协方差矩阵 $\boldsymbol{C}_{\text{p}}$ 的特征值组成的对角矩阵和对应的特征向量,$\boldsymbol{C}_{\text{p}}=\boldsymbol{E}\times\boldsymbol{\Lambda}\times\boldsymbol{E}^{\text{T}}$,利用先验知识和前向模型得到模拟方向反射率数据 $\boldsymbol{Y}_{\text{simu}}$,即 $\boldsymbol{Y}_{\text{simu}}=\boldsymbol{A}_{\text{simu}}\times\boldsymbol{X}_0$,其中 $\boldsymbol{A}_{\text{simu}}=\boldsymbol{\Lambda}^{-1/2}\times\boldsymbol{E}^{\text{T}}$,表示模拟数据观测方向的核矩阵,$\boldsymbol{y}_{\text{obs}}$ 在本研究中为 HJ-1 CCD 数据,n 为先验信息比,n 越小,先验知识在反演中所占的权重越高,反演结果越稳定,但也越接近于先验知识;相反,n 越大,观测数据所占的权重越高,反演结果越趋于不稳定。因此存在一个最佳值,可合理平衡先验知识与观测的权重,使得反演稳定,同时又使观测数据所包含信息最大程度地传递到待反演的参数。为了确定最佳的先验信息比,李小文等人(Li 等,2001)选取了一组典型的地表数据集,用全部观测数据反演得到的白天空反照率作为真实值,然后在数据集中选取一个观测,设定不同的先验信息比,对比反演结果与真实值的差异,多次重复实验后得出,当只有一个观察数据时,3/4 的先验信息比,对于地表观测能够给出稳定且又能反映地表真实参数的结果。在本研究中,我们根据地表类型赋予不同先验信息比,通过 HJ-1 卫星和 MODIS 的白天空反照率的对比发现,当 n 变化 1 时,会引起 HJ-1 卫星各波段白天空反照率约 0.02 的变化,当 $n\approx9$ 时,二者的白天空反照率最接近。

表 2 核驱动模型参数先验分布

参数	红波段			近红外波段		
	f_{iso}	f_{vol}	f_{geo}	f_{iso}	f_{vol}	f_{geo}
平均值	0.1064	0.0508	0.0159	0.2892	0.1721	0.0295
标准差	0.0108	0.0028	0.0006	0.0091	0.0054	0.0012
协方差矩阵 $\boldsymbol{C}_{\text{p}}$	0.00935 0.00137 0.00155 0.00137 0.00170 0.00034 0.00155 0.00034 0.00045			0.00773 0.00014 0.00160 0.00014 0.00959 −0.00235 0.00160 −0.00235 0.00145		

图 2 给出了两种应用先验知识反演地表反照率算法及比较流程,为了便于后期交叉验证,还计算了 HJ-1 卫星过境时基于地表朗伯假设的地表反照率和 MODIS 反照率。对于基于地表朗伯假设条件下的地表反照率,简单等于其方向反射率(Liang 等,2001),MODIS 反照率可以根据其产品获得。考虑地表时相变化的特征,我们选择研究区不同时相的 HJ-1 CCD 数据反演地表反照率,研究区时相特征可以通过 MODIS 地表物候产品(MCD12Q2)获得。对研究区的增强植被指数(EVI)的统计结果显示,研究区地表类型有明显物候期的变化,4 月中旬植被开始发芽进入生长期,到 7 月上旬植被进入成熟期,EVI 达到峰值,8 月下旬落叶林开始衰老、脱落。在 4 个物候期内,共选取 13 天云量少且能见度高的 HJ-1 CCD 数据进行地表反照率反演,并对典型物候的结果进行对比分析。

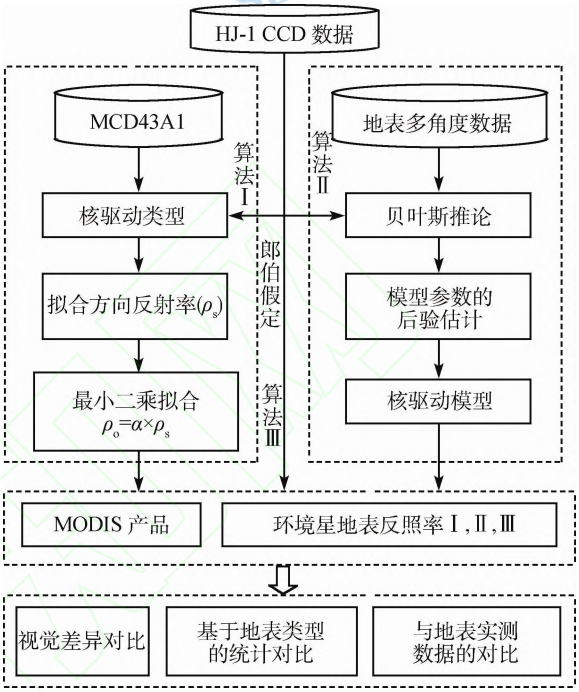

图 2 应用先验知识反演地表反照率算法及对比流程图

3 结果与分析

为验证反演结果的精度,对上述算法得到的 HJ-1 卫星地表反照率进行了评估。首先将算法Ⅰ和算法Ⅱ得到的真实地表反照率与 MODIS 产品进行目视效果对比;然后,计算不同地表类型的均值和方差,并与 MODIS 产品在统计意义上比较绝对和相对误差;最后将上述 3 种算法估算的结果分别和 MODIS 反照率产品及盈科气象站通量塔的地表观测数据和进行了比较。由于地表观测数据以及 HJ-1 CCD 数据是天空直射光和散射光的组合,为了和地表观测数据进行比较,我们考虑了大气状况,将黑白天空反照率根据式(2)转换成地表真实反照率(蓝天空反照率),最终转化成和地表观测数据波段范围相近的短波反照率进行比较,尽可能消除波谱分辨率差异对结果的影响。由于地表 73 组数据仅有红和近红外两个波段的观测,且 HJ-1 CCD 数据与 AVHRR 的波段范围相似,在窄波段到宽波段的转换过程中参考了 AVHRR 的转换系数(Liang 等,2003)。

3.1 反演结果图与统计

图 3 给出了 2009-08-14(植被生长旺盛时期)不同算法得到的黑河区域地表短波反照率分布图。图中依次列出了不同算法得到研究区地表反照率结果图以及部分区域的结果放大显示图，明显可以

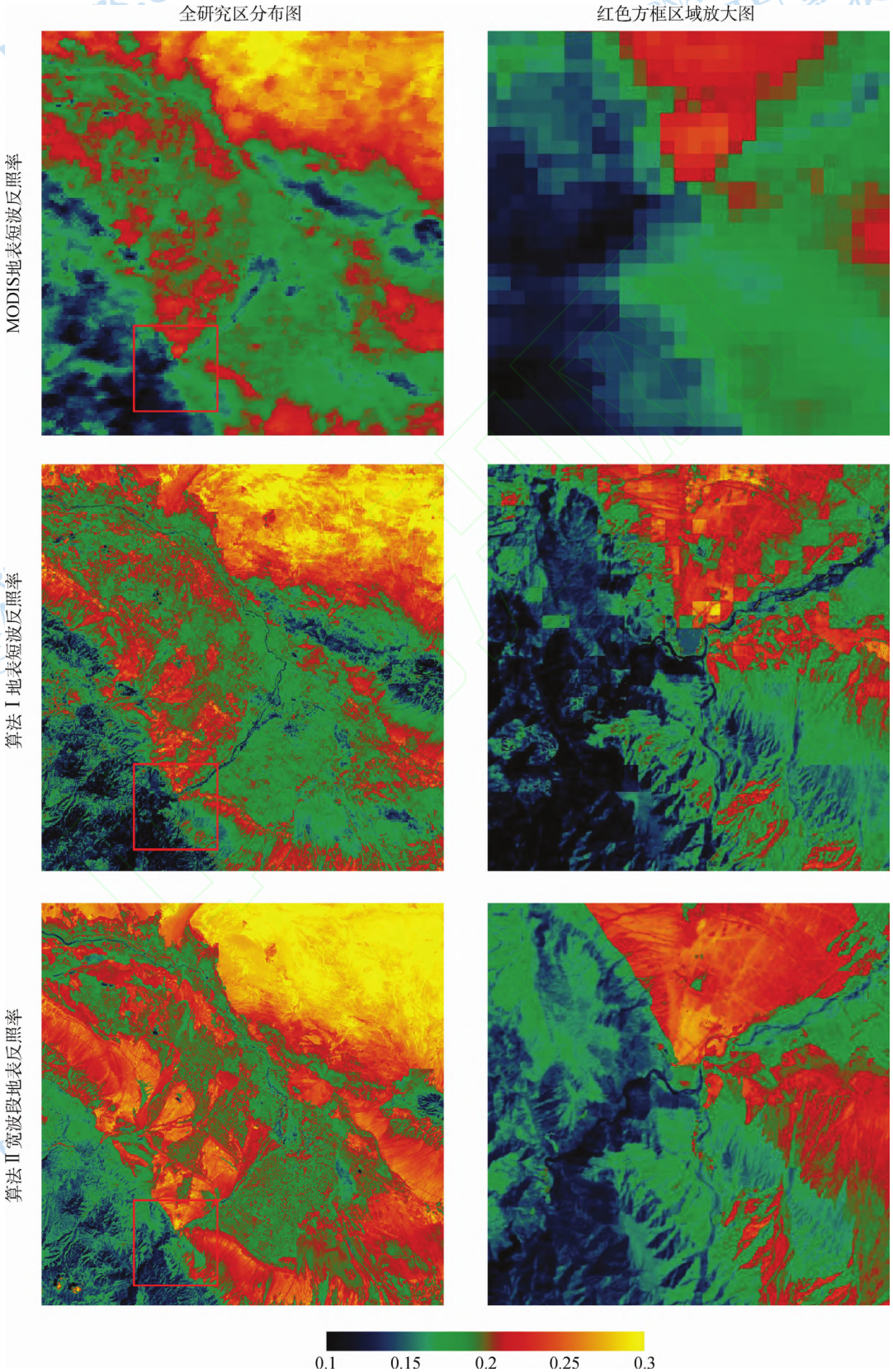

图 3 3 种算法得到的 2009-08-14 研究区地表反照率分布图

看出,MODIS 的反照率比较平滑,主要是因为它是混合像元内不同地表类型反照率的综合体现;两种基于先验知识得到的 HJ-1 卫星地表反照率和 MODIS 产品一样,都能够提供下垫面主要的空间分布特征,但基于先验知识的算法得到的 HJ-1 卫星地表反照率能提供更多的地表细部结构,比如放大结果图中间部分可以看到较窄的河流,左下角还可以看出对地形、地貌及地质构造等信息有较强的表现力。但是由于算法Ⅰ是在一个 500 m 的 MODIS 尺度应用同一先验知识,其结果中会出现马赛克现象,这种影响在地类破碎区域(类别交界处)表现最为显著,相比较而言,算法Ⅱ得到的地表反照率结果则表现得较为均匀。

图 4 给出了算法Ⅰ、算法Ⅱ、算法Ⅲ和 MODIS 短波反照率的均值和标准差(误差线,仅给出正值)。为说明不同算法结果的差异,将各算法在 4 个典型时相的不同地表类型的统计结果和 MODIS 反照率进行比较。和 MODIS 相比,基于先验知识的地表反照率较地表朗伯反演算法有不同程度的改善作用,地表朗伯条件下的反照率与 MODIS 反照率的绝对误差约为 0.03,相对误差约为 13%,而两种基于先验知识地表反照率结果和 MODIS 反照率产品更加接近,绝对误差约为 0.01,相对误差约为 4%。这两种算法对反照率的改善,对地表类型的依赖不明显,相对误差集中在 2%—8%。反照率精度改善不依赖于地表类型的特点,可能是由于地表 BRDF 的类内变化和类间变化的差异不明显(Jiao 等,2011),因此,建立一个基于 BRDF 变化的分类体系,可能更有助于 BRDF 作为地表先验知识的应用。地表先验知识对反照率估算的改善作用在不同程度上依赖于时相的变化,在植被最茂盛的季节改善作用明显强于凋谢季,以草地为例,4 月 4 日与 MODIS 的相对误差约为 7%,而 8 月 14 日相对误差不到 1%,这可能与植被在生长过程中表现出的不同的各向异性反射有关。

值得注意的是,部分时相中研究区内有零星云的污染,会对部分地表类型的反照率反演产生一定的影响。算法Ⅰ中虽然是相同时相的先验信息像元对像元的应用,但在一个 MODIS 像元下使用同一先验知识,通过观测数据调整先验的 BRDF 形状位置,实现对观测数据的 BRDF 校正,在数据空间中,先验的 BRDF 形状和数据为零拟合,造成观测数据误差 100% 传递到反照率的计算中。对于算法Ⅱ,对全部数据使用了相同的地表先验知识,通过先验信息比来调节先验知识在结果中所占的比重,部分克服了反照率反演结果中的误差传递问题。

通过以上比较和分析发现,基于地表先验知识的反照率算法,通过应用 HJ-1 CCD 单个角度反射

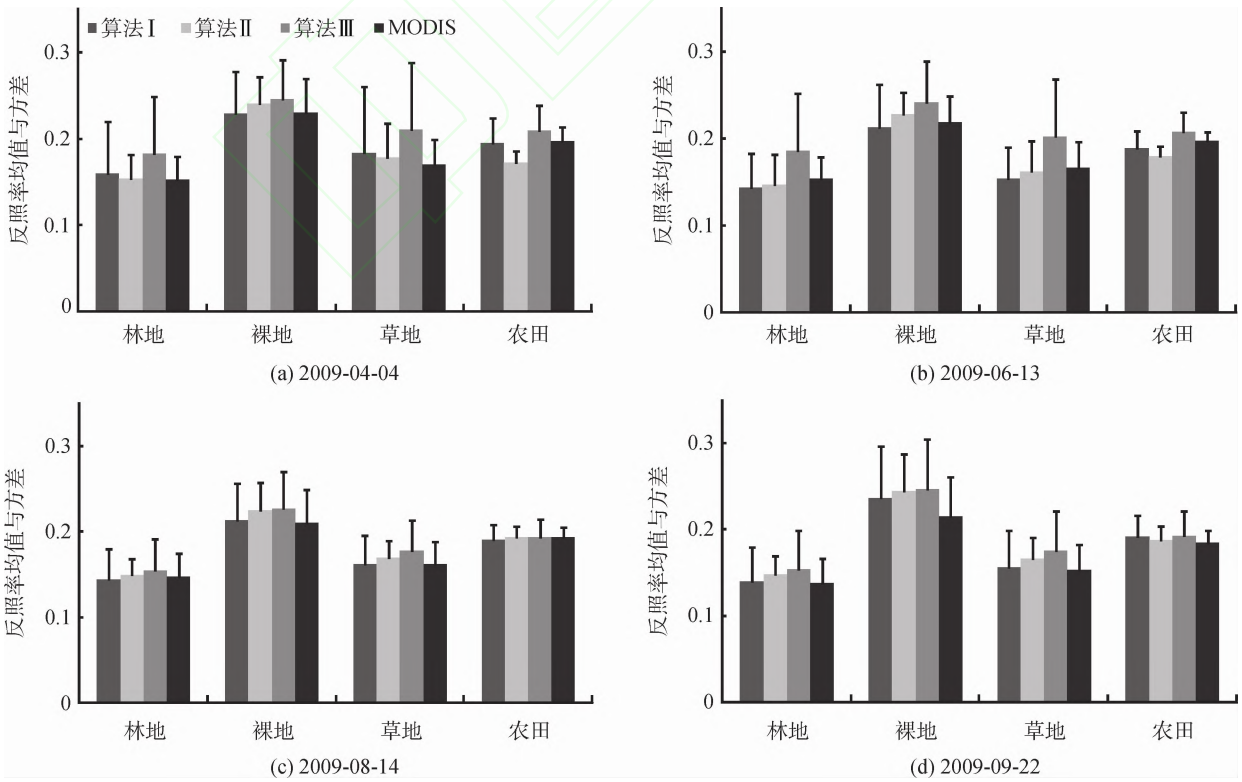

图 4 4 个时相,4 种典型地表类型,3 种算法及 MODIS 短波反照率的均值(柱状图)和标准差(误差线,仅给出正值)

率信号，相对于地表朗伯假设的传感器观测值，虽然提高了地表反照率的反演精度，但精度的改善在黑河实验区并不显著。为了进一步分析原因，以算法Ⅰ为例，在研究区内的 4 种典型地类中分别随机选取一个像元，绘制了 4 个不同时相在红波段下垫面先验 BRDF 形状(即 MODIS BRDF 形状)，以及对应 HJ-1 CCD 在相同时相下在该像元处的单角度观测的空间位置和反射率值(图 5 中的黑点)，从图 5 中热点的位置(红色区域)可以判断出太阳所在的位置。可以看出，随着时相的变化，观测位置和太阳位置并不固定，表现出一定变动，导致观测位置落在先验 BRDF 形状的反射率等高线位置有很大的变化，很多情况观测反射率接近于高反射的热点区域，如图 5 中 9 月份的林地。显然，以这个反射率的值代替朗伯假设条件下的反照率，相对于传统天顶方向的观测值，会明显提高地表的整体反照率。白天空反照率是双向反射率的积分(可认为是双向反射率的均值)，因此，对于 HJ-1 CCD 传感器而言，太阳和观测相对位置，可能会使地表朗伯假设条件下的地表反照率获得一个相对于天顶方向的一个较大的反照率值，从而导致算法Ⅰ相对于算法Ⅲ提高有限。

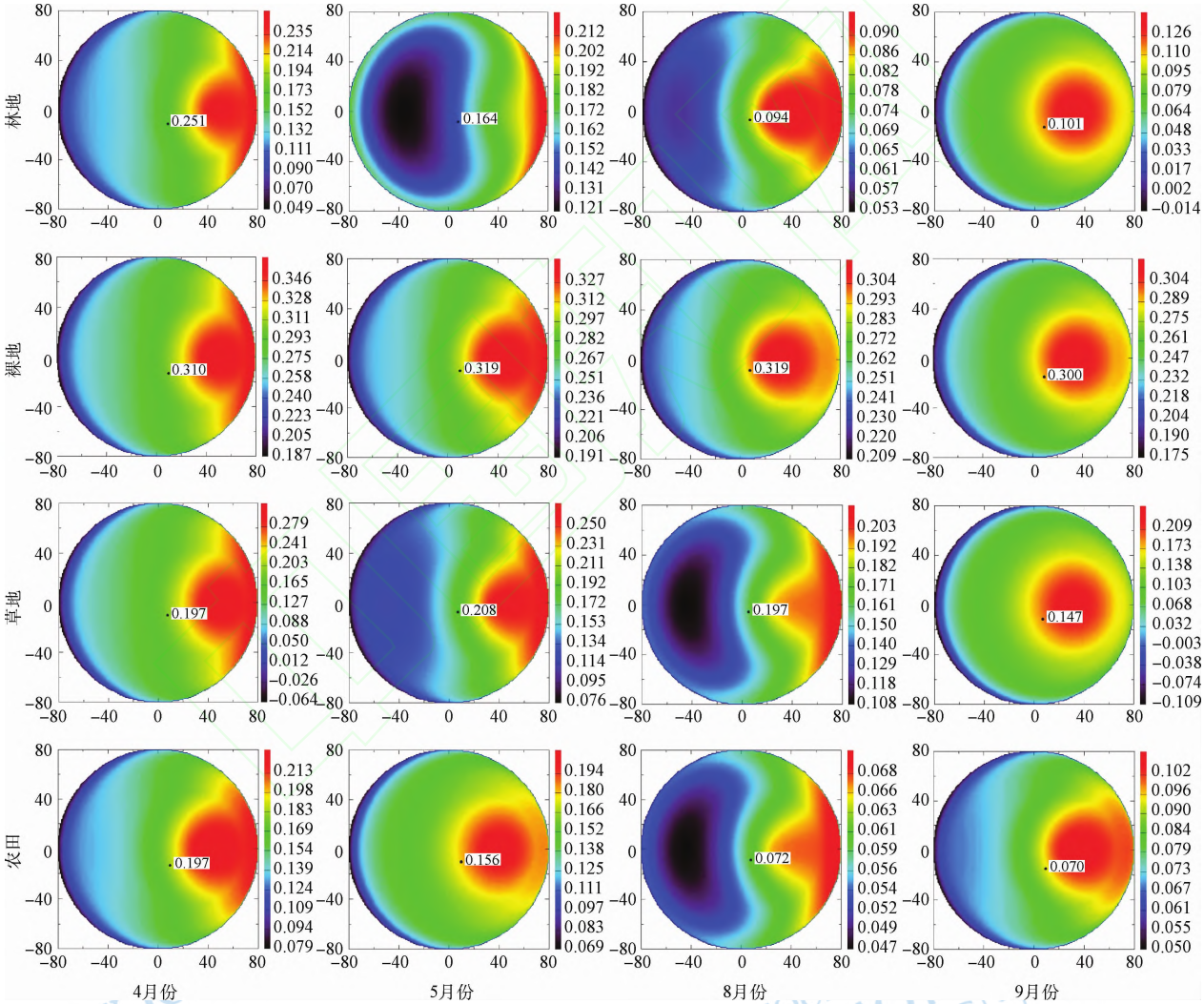

图 5　红波段 4 种地表类型在不同时相内 MODIS BRDF 示意图

(BRDF 形状以极坐标形式给出，中心为天顶方向，点到中心的距离表示天顶角的大小，极角代表方位角的大小，横纵坐标的正负值用于区分观测的前后向。黑点代表 HJ-1 的观测位置，同时也给出了相应的数值大小)

从图 5 中还可以看出，地表 BRDF 形状在不同地表类型和不同时相均存在较大差异。总体来讲，在 4 月份，植被处于凋谢期，地表的反射以裸地的反射为主，因此 4 月份所有地表先验的 BRDF 形状表现出显著的“屋顶状”，在热点方向呈现出一个显著的反射峰值。随着时相的变化，在 5 月份，林地和草地开始变绿，但田地可能尚未播种，因此田地和裸地还是以土壤的反射为主，仍然为“屋顶状”，但林

地和草地 BRDF 形状发生了不同程度的变化,开始呈现不同程度的“碗状”,存在较明显的 BRDF 光谱效应。到了 8 月份,除了裸地外,其他类型的 BRDF 形状呈现出不同程度的“碗状”,9 月份,除了田地外,BRDF 的形状基本和 4 月份保持一致,表明地表植被类型的 BRDF 形状完成一个完整的物候期,在整个时相的变化过程中,裸地的 BRDF 形状基本保持不变。在近红外波段也有相似的结果。

3.2 地表观测数据的验证

将遥感反演产品和地表实测数据相比较,是精度检验的重要一步。地表实测数据能够在一定程度上代表地面的真实情况,缺点是无法在卫星遥感尺度上进行地面观测。盈科灌区绿洲站自动气象站位于甘肃省张掖市的盈科灌区农田内,观测点的经纬度为 100°25′E,38°51′N,海拔高度为 1519 m,下垫面相对均一,观测数据具有代表性。为验证反演结果精度,可以将地面观测数据与卫星观测数据在不同的尺度下做有意义的比较(Liang 等,2003)。将各种算法反演的结果以及 MODIS 产品与地表观测数据进行比较,图 6 给出了各算法时间序列上的短波反照率与地表观测的比较结果。可以看出反照率有明显的季节特性,受叶片中色素的影响,在夏季的反照率较小。基于先验知识反演地表反照率及 MODIS 产品和地表观测有很好的一致性。对于算法Ⅰ来说与地表数据的绝对误差,除 181 天和 265 天外都在 0.02—0.05,平均绝对差异为 0.032,满足反照率精度要求;算法Ⅱ、算法Ⅲ和 MODIS 产品有分别有 5 天、4 天和 8 天不满足精度要求,平均绝对差异为 0.032、0.057 和 0.042。同时还可以看出 MODIS 反照率变化的季节性不明显(Schaaf,2002),这可能是由于 MODIS 混合像元的影响。

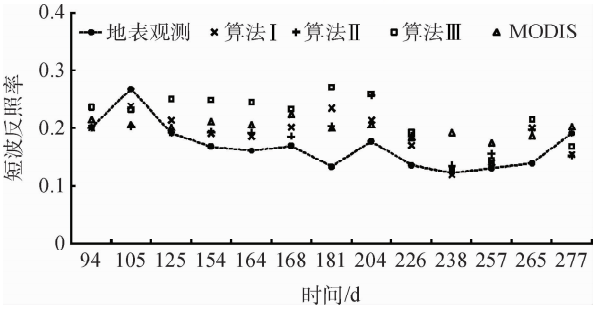

图 6 时间序列的 HJ-1 CCD 过境时盈科气象站不同算法反演地表短波反照率结果与地表通量塔观测数据对比图

图 7 给出了不同算法与地表观测对比散点图,算法Ⅰ、算法Ⅱ及 MODIS 产品与地表观测数据的均方根误差分别为 0.043、0.046 和 0.048,相对误差在 20% 左右,基于朗伯假定的算法Ⅲ与地表观测数据的均方根误差为 0.069,相对误差高达 36.3%。因此要精确估算地表反照率必须考虑地表的各向异性。

算法Ⅰ、算法Ⅱ及 MODIS 产品在很多情况下和地表观测结果较为一致,但有时也有明显的差异,造成这种现象的原因可能是:(1)BRDF 的尺度效应(Jin 等,2003),算法Ⅰ应用 MODIS 产品的 BRDF 形状作为先验知识,而 MODIS 粗分辨率和地表观测数据存在较为显著的尺度效应。算法Ⅱ对全部时像以及全部研究区应用了有限的地表观测作为的先验知识,这些观测大多数来源于同一时相观测,因此并没有考虑先验知识的时相差异。(2)HJ-1 CCD 数据质量的影响,算法Ⅰ中先验的 BRDF 形状和 HJ-1 CCD 数据为零拟合,算法Ⅱ中对通过先验信息比来调节先验信息和观测信息在结果中所占的比重,这两种算法的抗噪能力差,对观测数据的质量要求较高。

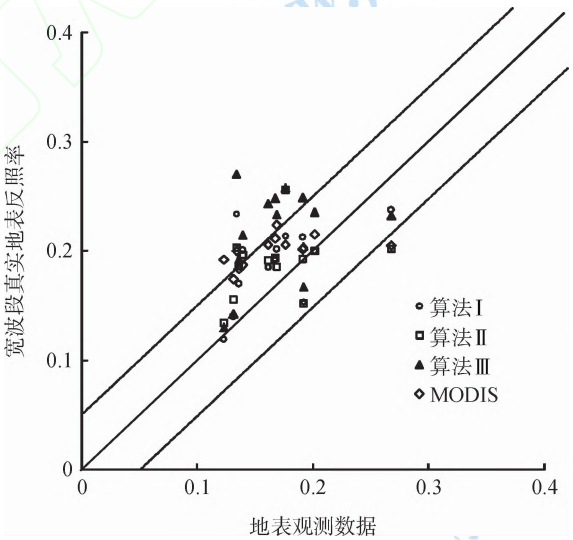

图 7 盈科气象站不同算法地表短波反照率的结果与地表通量塔观测数据对比散点图

4 结论与讨论

基于先验知识可以较好改善地表反照率反演精度,本文通过应用 HJ-1 CCD 数据对黑河实验区进行了 3 种算法的反照率反演和对比分析,这些算法包括基于 MODIS 业务化备用算法(算法Ⅰ)、基于贝叶斯原理的反照率反演算法(算法Ⅱ)和基于地表朗伯假设条件下直接应用 HJ-1 CCD 反射率数据代

表反照率(算法Ⅲ)。并将各算法结果及 MODIS 产品与地表观测数据进行比较，通过比较分析，得出了以下几点结论:

(1)两种基于先验知识得到的高分辨率的 HJ-1 CCD 地表反照率除提供下垫面主要的空间分布特征外，还能提供地表细部结构，但是由于算法Ⅰ在一个 500 m MODIS 像元下使用同一 BRDF 形状作为先验知识，在结果中会出现马赛克现象，这种影响在地表类型破碎区域表现尤为显著。相比较而言，算法Ⅱ表现的较为均匀。

(2)在星载多角度观测数据缺乏的情况下，引入地表各向异性的先验知识，可以有效改善地表反照率的反演精度。不同地表类型的统计表明，和 MODIS 产品相比，基于朗伯假定的地表反照率算法的绝对误差为 0.03，相对误差为 13%；而基于先验知识反演的结果绝对误差为 0.01，相对误差为 4%。

(3)对于 HJ-1 CCD 而言，算法Ⅰ和算法Ⅱ相对于 MODIS 反照率产品在统计意义上对改善地表反照率的反演精度相似，算法Ⅰ与算法Ⅱ和地表观测数据相比，绝对误差小于 0.05，相对误差小于 23%；而算法Ⅲ的误差为 0.069，相对误差为 36.3%，这与 Kimes(1985)的早期结果较为接近。在黑河实验区内，算法Ⅰ优于算法Ⅱ，MODIS 产品再次之，算法Ⅲ最差。算法Ⅰ通过相同时相 MODIS 粗分辨率的 BRDF 形状作为先验知识，是像元对像元的应用，但是受尺度的影响较显著。算法Ⅱ中对全部数据仅使用有限的地表观测数据作为先验知识，通过先验信息比来调节先验知识在结果中所占的比重，先验信息相对不足。

(4)不同算法对反照率的改善，对地表类型的依赖不明显，相对误差集中于 2%—8%。在不同程度上依赖于时相的变化，在植被最茂盛的季节，改善作用明显强于凋谢季，这可能与植被在生长过程中表现出的不同各向异性反射有关。

(5)对于单个观测角度，MODIS 备用算法的主要限制可能在于对先验的 BRDF 形状的“硬调整”，因而受单个观测的误差影响大，如果采用 2 个以上观测的情况，应用该算法可能会更有效。目前，这种思想已在 MODIS 第 5 版以后的反照率业务化备用算法中被采用。

以上两种基于先验知识的反照率反演算法，可能会依赖于传感器的成像方式、区域位置以及地表类型和时相。这是因为，不同传感器的成像方式会决定太阳和观测几何的相对位置，因此影响到对先验 BRDF 形状的调整；而区域位置和时相变化会影响太阳几何；此外，不同地表类型的 BRDF 形状变化也有待进一步研究。因此，以中国地区为研究区域，寻找和应用一个基于 BRDF 形状的分类体系，通过建立典型地表类型 BRDF 先验知识库，更有效地利用 BRDF 先验知识，是我们今后工作的重点。

志　谢　基于贝叶斯推论算法得到了北京师范大学地理与遥感科学学院杨华老师的帮助，CCD 图像数据的获取得到资源卫星应用中心相关部门的支持，地表通量数据来源于国家自然科学基金委员“中国西部环境与生态科学数据中心”，在此表示衷心感谢！

参考文献(References)

Deering D and Leone P. 1986. A sphere-scanning radiometer for rapid directional measurements of sky and ground radiance. Remote Sensing of Environ, 19(1): 1-24 [DOI: 10.1016/0034-4257(86) 90038-6]

Dickinson R E. 1995. Land processes in climate models. Remote Sensing of Environment, 51(1): 27-38 [DOI: 10.1016/0034-4257(94) 00062-R]

杜鑫, 陈雪洋, 蒙继华, 张飞飞, 张森, 吴炳方. 2010. 基于6S 模型的环境星 CCD 数据大气校正. 国土资源遥感, 21(2): 22-25

Du X, Chen X Y, Meng J H, Zhang F F, Zhang M and Wu B F. 2010. Atmospheric correction of HJ-1 CCD data based on 6S model. Remote Sensing for Land and Resources, 21(2): 22-25

Eidenshink J C and Faundeed J L. 1994. The 1-km AVHRR global land data set: first stages in implementation. International Journal of Remote Sensing, 15(17): 3443-3462 [DOI: 10.1080/01431169408954339]

Hu B X, Lucht W G, Li X W and Strahler A H. 1997. Validation of kernel-driven semiempirical models for the surface bidirectional reflectance distribution function of land surfaces. Remote Sensing of Environment, 62(3): 201-214 [DOI: 10.1016/S0034-4257(97) 00082-5]

Irons J R, Campbell G S, Norman J M, Graham D W and Kovalick W M. 1992. Prediction and measurement of soil bidirectional reflectance. IEEE Transactions on Geoscience and Remote Sensing, 30(2): 249-260 [DOI: 10.1109/36.134075]

Jiao Z T, Li X W, Wang J D and Zhang H. 2011. Assessment of MODIS BRDF shape indicators. Journal of Remote Sensing, 15(3): 432-456

Jin Y F, Schaaf C B, Gao F, Li X W, Strahler A H, Lucht W and Liang S L. 2003. Consistency of MODIS surface bidirectional reflectance distribution function and Albedo retrieval: 1. Algorithm Performance. Journal of Geophysical Research, 108(D5): 4158 [DOI: 10.1029/2002JD002803]

Kimes D S and Seller P J. 1985. Inferring hemispherical reflectance of the Earth's surface for global energy budgets from remotely-sensed

nadir or directional radiance values. Remote Sensing Environment, 18(3): 205-223 [DOI: 10.1016/0034-4257(85)90058-6]

Kimes D S, Newcomb W W, Nelson R F and Schutt J B. 1986. Directional reflectance distributions of a hardwood and pine forest canopy. IEEE Transactions on Geoscience and Remote Sensing, 24 (2): 281-293 [DOI: 10.1109/TGRS.1986.289647]

Leroy M and Breon F M. 1996. Surface reflectance angular signatures from airborne POLDER data. Remote Sensing Environment, 57: 97-107

Lewis P and Barnsley M J. 1994. Influence of the sky radiance distribution on various formulations of the earth surface albedo. Proceedings of Conference on Physical Measurements of Signatures in Remote Sensing, Courchevel, France. International Society for Photogrammetry and Remote Sensing: 707-715

Li X W, Gao F, Wang J D and Strahler A H. 2001. A priori knowledge accumulation and its application to linear BRDF model inversion. Journal of Geophysics Research, 106(D11): 11925-11935 [DOI: 10.1029/2000JD900639]

李小文, 王锦地, 胡宝新, Strahler A H. 1998. 先验知识在遥感反演中的作用. 中国科学, D 辑, 28(1): 67-72

Li X W, Wang J D, Hu B X and Strahler A H. 1998. Application of Priori knowledge in remote sensing inversion. Science China (Series D), 28(1): 67-72

Liang S L. 2001. Narrowband to broadband conversions of land surface albedo: I. algorithms. Remote Sensing of Environment, 76(2): 213-238 [DOI: 10.1016/S0034-4257(00)00205-4]

Liang S L, Fang H L, Chen M Z, Shuey C J, Walthall C, Daughtry C, Morisette J, Schaaf C and Strahler A. 2002. Validating MODIS land surface reflectance and albedo products: methods and preliminary results. Remote Sensing of Environment, 83(1/2): 149-162 [DOI: 10.1016/S0034-4257(02)00092-5]

Liang S L, Shuey C J, Russ A L, Fang H L, Chen M Z, Walthall C L, Daughtry C S T and Hunt R. 2003. Narrowband to broadband conversions of land surface albedo: II. Validation. Remote Sensing of Environment, 84(1): 25-41 [DOI: 10.1016/S0034-4257(02)00068-8]

Liu J C, Schaaf C, Strahler A, Jiao Z, Shuai Y M, Zhang Q L, Roman M, Augustine J A and Dutton E G. 2009. Validationof moderate resolution imaging spectroradiometer (MODIS) albedo retrieval algorithm: dependence of albedo on solar zenith angle. Journal of Geophysical Research, 114(D1): D01106 [DOI: 10.1029/2008JD009969]

Lucht W, Schaaf C B and Strahler A H. 2000. An algorithm for the retrieval of albedo from space using semiempirical BRDF models. IEEE Transactions on Geoscience and Remote Sensing, 38(2): 977-998 [DOI: 10.1109/36.841980]

马明国, 王维真, 黄广辉, 张智慧, 谭俊磊. 2008. 黑河综合遥感联合试验: 盈科灌区绿洲站自动气象站数据集

Ma M G, Wang W Z, Huang G H, Zhang Z H and Tan J L. 2008. WATER: Dataset of automatic meteorological observations at the Yingke oasis station. Cold and Arid Regions Environmental and Engineering Research Institute. Chinese Academy of Sciences

Nicodemus F E, Richmond J C, Hsia J J, Ginsberg W I and Limperis T. 1977. Geometrical Considerations and Nomenclature for Reflectance. Washington, DC: Institute for Basic Standards, NBS MN-160

Pokrovsky O and Roujean J L. 2002. Land surface albedo retrieval via kernel-based BRDF modeling: statistical inversion method and model comparison. Remote Sensing Environment, 84(1): 100-119 [DOI: 10.1016/S0034-4257(02)00100-1]

Ranson K J, Biehl L L and Bauer M E. 1985. Variation in spectral response of soybeans with respect to illumination, view and canopy geometry. International Journal of Remote Sensing, 6(12): 1827-1842 [DOI: 10.1080/01431168508948331]

Rodgers C D. 1976. Retrieval of atmospheric temperature and composition from remote measurements of thermal radiation. Reviews of Geophysics, 14(4): 609-624 [DOI: 10.1029/RG014i004p00609]

Roujean J L, Leroy M and Deschamps P Y. 1992. A bidirectional reflectance model of the earth's surface for the correction of remote sensing data. Journal of Geophysical Research, 97(D18): 20455-20468 [DOI: 10.1029/92JD01411]

Salomon J G, Schaaf C B, Strahler A H, Gao F and Jin Y F. 2006. Validation of the MODIS bidirectional reflectance distribution function and albedo retrievals using combined observations from the aqua and terra platforms. IEEE Transactions on Geoscience and Remote Sensing, 44(6): 1555-1565 [DOI: 10.1109/TGRS.2006.871564]

Schaaf C B, Gao F, Strahler A H, Lucht W, Li X W, Tsang T, Strugnell N C, Zhang X Y, Jin Y Y, Muller J P, Lewis P, Barnsley M, Hobson P, Disney M, Roberts G, Dunderdale M, Doll C, d'Entremont R P, Hu B X, Liang S L, Privette J L and Roy D. 2002. First operational BRDF, Albedo Nadir reflectance products from MODIS. Remote Sensing of Environment, 83(1/2): 135-148 [DOI: 10.1016/S0034-4257(02)00091-3]

Schaaf C L B, Liu J, Gao F and Strahler A H. 2011. MODIS albedo and reflectance anisotropy products from Aqua and Terra, land remote sensing and global environmental change // Ramachandran B, Justice C, Abrams M, eds. NASA's Earth Observing System and the Science of ASTER and MODIS, Remote Sensing and Digital Image Processing Series, Vol. 11. New York: Springer-Cerlag: 873 [DOI: 10.1016/j.rse.2011.04.019]

Shuai Y M, Masek J G, Gao F and Schaaf C B. 2011. An algorithm for the retrieval of 30-m snow-free albedo from Landsat surface reflectance and MODIS BRDF. Remote Sensing of Environment, 115(9): 2204-2216 [DOI: 10.1016/j.rse.2011.04.019]

Strugnell N and Lucht W. 2001. An algorithm to infer continental-scale albedo from AVHRR data, land cover class and field observations of typical BRDF's. Journal of Climate, 14: 1360-1376

Strugnell N C, Lucht W and Schaaf C. 2001. A global albedo data set derived from AVHRR data for use in climate simulations. Geophysical Research Letters, 28(1): 191-194 [DOI: 10.1029/2000GL011580]

孙源, 顾行发, 余涛, 高海亮.2010. 环境星 CCD 数据大气校正研究. 国土资源遥感, 87(4): 6-9

Sun Y, Gu X F and Yu T. 2010. A study of HJ-1A CCD image atmospheric correction. Remote Sensing for Land and Resources, 87(4): 6-9

Tarantola A. 1987. Inverse Problem Theory: Methods for Data Fitting and Model Parameter Estimation. New York: Elsevier Science: 613

Tsay S C, King M D, Arnold G T and Li J Y. 1998. Airborne spectral

measurements of surface anisotropy during SCAR-B, Journal of Geophysical Research, 103(D24): 31943－31953［DOI: 10.1029/98JD01167］

Wang Y F, Li X W, Nashed Z, Zhao F, Yang H, Guan Y N and Zhang H. 2007. Regularized kernel based BRDF model inversion method for ill-posed land surface parameter retrieval. Remote Sensing of Environment, 111(1): 36－50［DOI: 10.1016/j.rse.2007.03.007］

王锦地, 张立新, 柳钦火, 张兵, 尹球. 2009. 中国典型地物波谱知识库. 北京: 科学出版社

Wang J D, Zhang L X, Liu Q H, Zhang B and Yin Q. 2009. The spectrum database of typical objects in China. Beijing: Science Press：231－290

Wanner W, Li X W and Strahler A H. 1995. On the derivation of kernels for kernel-driven models of bidirectional reflectance. Journal of Geophysical Research, 100(D10): 21077－21090［DOI: 10.1029/95JD02371］

杨华, 许王莉, 赵红蕊, 陈雪, 王锦地. 2003. 定量遥感正则化反演中的信息流及其控制. 中国科学, 33(8): 799－808

Yang H, Xu W L, Zhao H R, Chen X and Wang J D. 2003. Information stream and its control in the inversion of Quantitative remote sensing regularization of inversion. Science in China (Series D), 33(8): 799－808